Journal of Structural Geology 100 (2017) 98–119

Contents lists available at ScienceDirect

Journal of Structural Geology

journal homepage: www.elsevier.com/locate/jsg

Complex fold and thrust belt structural styles: Examples from the Greater Juha area of the Papuan Fold and Thrust Belt, Papua New Guinea

Luke Mahoney [a, *], Kevin Hill [b], Sandra McLaren [a], Amanda Hanani [b]

[a] School of Earth Sciences, The University of Melbourne, VIC, 3010, Australia
[b] Papuan Oil Search Ltd, Sydney, NSW, 2000, Australia

ARTICLE INFO

Article history:
Received 9 February 2017
Received in revised form
5 May 2017
Accepted 23 May 2017
Available online 25 May 2017

Keywords:
Fold and thrust belt
Structural style
Basin inversion
Arc-normal structures
Papua New Guinea
Papuan basin

ABSTRACT

The remote and inhospitable Papuan Fold Belt in Papua New Guinea is one of the youngest yet least well-documented fold and thrust belts on Earth. Within the frontal Greater Juha area we have carried out >100 km of geological traverses and associated analyses that have added significantly to the contemporary geological and geophysical dataset. Our structural analysis provides evidence of major inversion, detachment and triangle zone faults within the uplifted Eastern Muller Ranges. We have used the dataset to develop a quasi-3D model for the Greater Juha area, with associated cross-sections revealing that the exposed Cenozoic Darai Limestone is well-constrained with very low shortening of 12.6–21.4% yet structures are elevated up to 7 km above regional. We suggest the inversion of pre-existing rift architecture is the primary influence on the evolution of the area and that structures link to the surface via triangle zones and detachment faults within the incompetent Mesozoic passive-margin sedimentary sequence underlying competent Darai Limestone. Arc-normal oriented structures, dominantly oblique dextral, up-to-the-southeast, are pervasive across a range of scales and are here interpreted to relate at depth to weakened pre-existing basement cross-structures. It is proposed that Palaeozoic basement fabric controlled the structural framework of the basin during Early Mesozoic rifting forming regional-scale accommodation zones and related local-scale transfer structures that are now expressed as regional-scale arc-normal lineaments and local-scale arc-normal structures, respectively. Transfer structures, including complexly breached relay ramps, utilise northeast-southwest striking weaknesses associated with the basement fabric, as a mechanism for accommodating displacement along major northwest-southeast striking normal faults. These structures have subsequently been inverted to form arc-normal oriented zones of tear faulting that accommodate laterally variable displacement along inversion faults and connected thrust structures.

1. Introduction

Globally, there has been significant effort to document structural styles within fold and thrust belts, revealing often complex relationships between basin evolution and the subsequent style of deformation during compression. Early basin extensional architecture and mechanical stratigraphy appear to be key controls on the subsequent evolution of both thick- and thin-skinned compressional deformation. But modern rift and rifted-margin structural analogues show that extensional architecture is often remarkably complex (e.g., East African Rift: Morley et al., 1990; Chorowicz, 2005; North West Shelf, Australia: Longley et al., 2002; Frankowicz and McClay, 2010) and a wide range of factors impact inversion geometry and style (e.g., Buchanan and Buchanan, 1995; Bonini et al., 2012). Additionally, compression may occur in the presence of an evolving stress field associated with far- and near-field tectonism (e.g., Saintot and Angelier, 2002) or syn-tectonic sedimentation (e.g., Storti and McClay, 1995). For these reasons the relative influence of extension-related architecture and compression-related influences can be difficult to demonstrate, particularly where robust constraints on subsurface geometry are absent.

The Papuan Fold Belt (PFB) of Papua New Guinea (PNG) is

* Corresponding author.
E-mail address: luke.g.mahoney@gmail.com (L. Mahoney).

http://dx.doi.org/10.1016/j.jsg.2017.05.010
0191-8141/

located on the northern margin of the Australian plate (Fig. 1a) and has significant demonstrated mineral and hydrocarbon wealth. Yet the PFB remains poorly understood geologically, due largely to its isolation and its complex tectonic history. As such, it has the potential to provide significant new insights into our understanding of fold belts globally.

Over the past few decades, the accessibility and affordability of aviation-based exploration as well as new specialized methods of data acquisition (e.g., Hornafius and Denison, 1993; Hill et al., 1996a) have significantly improved our understanding of the local-scale structure of the PFB. Indeed the PFB is currently being actively explored for hydrocarbons and minerals involving drilling and the acquisition of widely-spaced 2D seismic data which substantially constrain geologic models. Moreover, recent and ongoing tectonism in the PFB means that present day convergence vectors (e.g., Wallace et al., 2004; Koulali et al., 2015; Stanaway and Noonan, 2015), earthquake solutions (e.g., Abers and McCaffrey, 1988; Ekström et al., 2012) and contemporary landforms can aid structural and tectonic models.

Significant variations in structural style have been recognised across the PFB, often related to pre-compression margin architecture (e.g., Hill, 1991; Buchanan and Warburton, 1996; Hill et al., 2010). However the majority of studies are based on cross-sections and do not explain how along-strike structural variations are accommodated. In particular, our understanding of the structure of the PFB decreases significantly to the west of the extensively explored hydrocarbon-bearing frontal structures in the Kutubu Fold and Thrust Belt (KFTB) (Fig. 1b). The remote neighbouring North West Fold and Thrust Belt (NWFTB) is characterised by a contrasting set of structural styles to that of the KFTB. Most obviously, it is characterised by comparatively higher surface elevations and broader structural wavelengths (Fig. 1b). Within the NWFTB region, the Greater Juha area (Fig. 1c) is contiguous with the PFB frontal hydrocarbon trend and is thus a highly prospective area undergoing active exploration. Indeed, the Juha Anticline and the Hides Anticline, 30 km further east, are both large gasfields (Fig. 1c).

Here, new geological field observations together with legacy data have been used to construct cross-sections and a detailed geological map to document and understand structural styles within the Greater Juha area of the NWFTB. Our contemporary dataset reveals a complex interplay of pre-compression rift architecture, mechanical stratigraphy and compressive stresses on the spatio-temporal evolution of the Greater Juha area.

2. Geological setting

The geological evolution of New Guinea is complex and much-debated, with a number of key tectonic events having had significant influence on the rock record. At present, the island of New Guinea comprises three major tectonic provinces (after Hill and Hall, 2003): (1) the Stable Platform to the south, (2) the Mobile Belt to the north and (3) the central New Guinea Fold Belt (NGFB) (Fig. 1a). The Stable Platform is the northern edge of the relatively undeformed Australian continent while the Mobile Belt comprises island arcs and microcontinents accreted to the leading edge of the Australian plate during the Cenozoic (e.g., Hill and Raza, 1999). The NGFB separates the Stable Platform and Mobile Belt and formed predominantly within sediments of the Australian continental margin during the Late Miocene to Pliocene (Hill and Gleadow, 1989).

2.1. Tectonic and stratigraphic framework

The rock record of New Guinea (Fig. 2) reveals a complex geological evolution for the northern margin of the Australian continent, which is summarised briefly here. Further details and tectonic history reconstructions for New Guinea are given in Pigram and Symonds (1991), Hill and Raza (1999), Hill and Hall (2003) and Baldwin et al. (2012) and for SE Asia by Hall (1996, 1997, 2002, 2012), Metcalfe (2002) and Zahirovic et al. (2014, 2016).

Limited basement outcrop and well intersections suggest Late Permian and Early Triassic metasediments and volcanics, and Middle to Late Triassic granites underlie most of the PFB and the Stable Platform within PNG (Fig. 1b). The overlying Mesozoic stratigraphic sequence was subsequently attributed to the tectonic stages of rift-drift sequences and facilitated early ideas for Early Mesozoic rifting on the New Guinea margin (e.g., Pigram and Panggabean, 1984). Northwest-southeast and WNW-ESE oriented grabens filled with Early Mesozoic syn-rift sediments (Fig. 2) and associated normal faults have been suspected to underlie the PFB (e.g., Hill, 1991) and have been identified across adjacent foreland regions (e.g., Home et al., 1990; Kawagle and Meyers, 1996; Schofield, 2000). The cessation of rifting in the Middle Jurassic was recorded throughout the Papuan Basin as a thick, widespread post-rift sequence dominated by fine-grained clastic sediments including the Jurassic-aged Imburu mudstone and Cretaceous-aged Ieru Formation (Fig. 2). During the early post-rift phase a number of prograding sandstone sequences were deposited, including the Early Cretaceous Toro Sandstone and Middle to Late Jurassic Koi Iange Sandstone (Fig. 2). Several of these sandstones host the main hydrocarbon reserves in the PFB. The Late Cretaceous to Palaeogene history of the Papuan Basin is largely unknown with a prominent top Ieru unconformity located across most of southern PNG (Fig. 2). Subsequent subsidence during the Late Oligocene to Early Miocene accommodated the deposition of 1–2 km of Darai Limestone (Fig. 2) in southern New Guinea, building the Cenozoic platform.

Compression within the Mobile Belt began during the Middle to Late Miocene (12–14 Ma) and within the NGFB in the Late Miocene to Pliocene (5-4 Ma) (Hill and Gleadow, 1989; Hill and Raza, 1999). The dominant orientation for compression-related structures throughout the PFB reflects northeast-southwest compression, with an increasingly large sinistral strike-slip component recognised northwards in the Mobile Belt (e.g., Pigott et al., 1985; Crowhurst et al., 1997), related to east-west compressive stresses from the ongoing collision with the Finisterre Arc terrane (Hill and Raza, 1999). Contemporary seismicity suggests the PFB is still undergoing compressive deformation with focal mechanisms suggesting northeast-southwest directed convergence (Ekström et al., 2012). In fact, GPS plate velocities suggest that the PFB may be accommodating up to 15 mm of convergence between the New Guinea Highlands (Mobile Belt) and Australian plate (Stable Platform) annually (Wallace et al., 2004; Koulali et al., 2015; Stanaway and Noonan, 2015).

In the Late Miocene, crustal flexure associated with plate collision and Mobile Belt uplift resulted in the formation of foreland basins to the south and southwest of the Papuan Highlands (e.g., Davies, 1983). This prompted the deposition of variably thick Late Miocene to present, shallow marine to non-marine syn-tectonic sediments. The onset of Late Miocene uplift is recorded by the deposition of calcareous clastics and reworked limestone fragments in the Orubadi Formation (Fig. 2) (Home et al., 1990). In the Pliocene, the progression of uplift and erosion in the highlands, along with contemporary volcanism, contributed to the deposition of the thick non-marine Era and Strickland Formations in the southwest of the PFB (Fig. 2) (Davies, 1983; Home et al., 1990).

Prominent stratovolcanoes and associated intrusions throughout PNG are, in general, poorly understood. Potassium-argon (K-Ar) data suggests that volcanism in the Papuan Highlands had begun by at least the Middle Miocene (Page, 1976). However, the majority of the prominent stratovolcanoes and

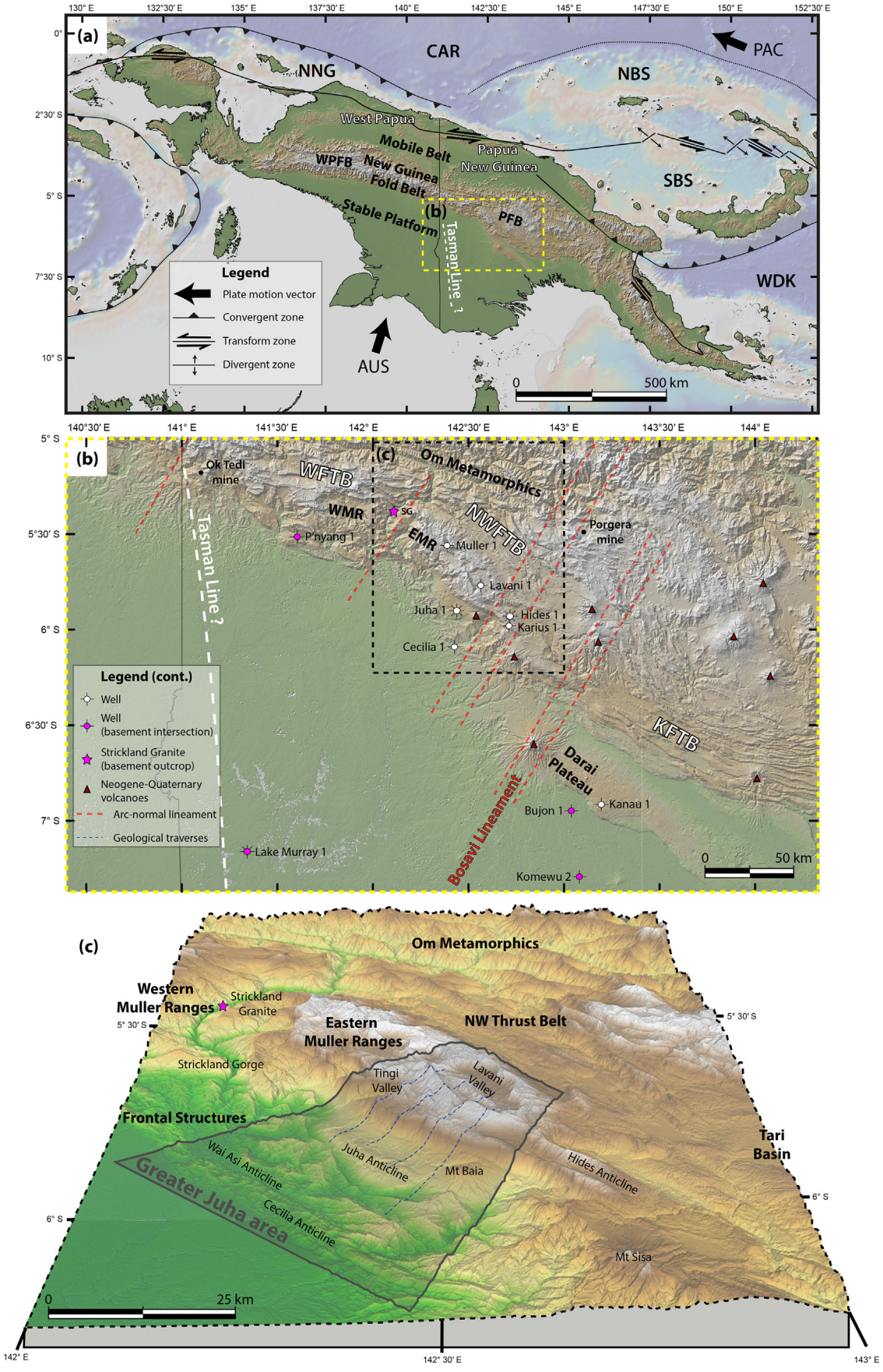
(a)
CAR
PAC
NNG
NBS
West Papua
Mobile Belt
Papua New Guinea
WPFB
New Guinea Fold Belt
SBS
Stable Platform
(b)
PFB
Tasman Line ?
WDK
Legend
Plate motion vector
Convergent zone
Transform zone
Divergent zone
AUS
0
500 km
(b)
Ok Tedi mine
WFTB
(c)
Om Metamorphics
WMR
SG
NWFTB
P'nyang 1
EMR
Muller 1
Porgera mine
Lavani 1
Juha 1
Hides 1
Karius 1
Cecilia 1
Tasman Line ?
Legend (cont.)
Well
Well (basement intersection)
Strickland Granite (basement outcrop)
Neogene-Quaternary volcanoes
Arc-normal lineament
Geological traverses
KFTB
Darai Plateau
Bujon 1
Kanau 1
Bosavi Lineament
Lake Murray 1
Komewu 2
0
50 km
(c)
Om Metamorphics
Western Muller Ranges
Strickland Granite
Eastern Muller Ranges
NW Thrust Belt
Strickland Gorge
Tingi Valley
Lavani Valley
Frontal Structures
Tari Basin
Wai Asi Anticline
Juha Anticline
Mt Baia
Hides Anticline
Greater Juha area
Cecilia Anticline
Mt Sisa
0
25 km

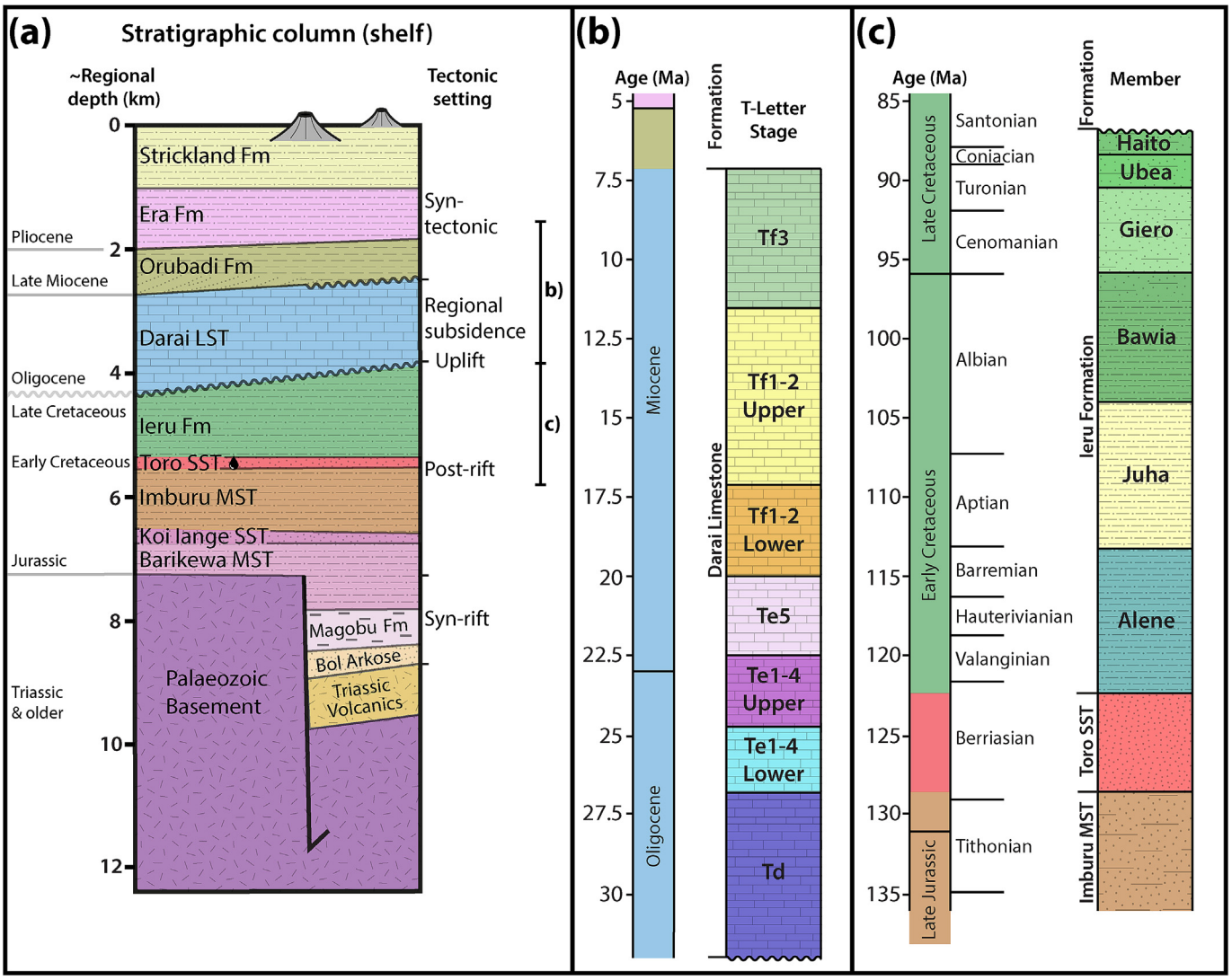

Fig. 2. Schematic stratigraphy of the Papuan Fold Belt (a) true stratigraphic thicknesses (TSTs) estimated from seismic and well data across the foreland of the Greater Juha area; (b) subdivision of the Darai Limestone into T-Letter stages (following Lunt and Allan, 2004) as used here; (c) subdivision of the Ieru Formation (following Bradley, 2014) as used here. Note the thickness of syn-tectonic sediments is based on foreland thicknesses and compaction modelling from the Juha Anticline (Hanani et al., 2016); thickness and extent across the EMR is unknown due to Plio-Pleistocene uplift and erosion.

associated intrusions within the PFB and on the Stable Platform formed during the Plio-Pliestocene (Webb, 1973; Löffler et al., 1979).

2.2. Structural styles

The NGFB is characterised by variations in structural style along its length from the wide Kutubu Fold and Thrust Belt (KFTB) to the comparatively narrow, highly elevated West Papuan Fold Belt (WPFB) (Fig. 1a). Structural variations on the scale of the entire NGFB are most commonly attributed to the transition from hot, weak Late Palaeozoic lithosphere in the east, to cold, strong Proterozoic lithosphere in the west, apparently coincident with the Tasman Line (Hill and Hall, 2003).

Diverse structural styles within the PFB have previously been attributed to the relative role of thin- and thick-skinned tectonics (e.g., Hill et al., 2000, 2010). Structures observed at the surface within Darai Limestone are commonly detached within thick, incompetent underlying sediments. For instance, Hill et al. (2010) recognised multiple major detachment levels across the KFTB including within the Ieru Formation and Imburu/Barikewa Mudstones. Basement-involved faulting within the PFB has often been

Fig. 1. **(a)** Tectonic components of New Guinea and the New Guinea Fold Belt. Tectonic elements modified from Hill and Hall (2003) and Baldwin et al. (2012). Trajectory of Tasman Line based on extent of Palaeozoic basement in outcrop and wells (see Fig. 1b). AUS, Australian plate; CAR, Caroline microplate; NBS, North Bismark plate; NNG; Northern New Guinea block; PAC, Pacific plate; PFB, Papuan Fold Belt; SBS, South Bismark plate; WDK, Woodlark microplate; WPFB, West Papuan Fold Belt. Yellow box indicates the location of Fig. 1b. **(b)** Structural elements of the PFB including arc-normal lineaments and locations of Late Palaeozoic-Early Mesozoic basement within the Strickland Gorge and wells across the foreland and PFB. Arc-normal lineaments based on Hill (1991) and Hill et al. (2000, 2002). EMR, Eastern Muller Ranges; KFTB, Kutubu Fold and Thrust Belt; NWFTB, North West Fold and Thrust Belt; SG, Strickland Granite; WFTB, Western Fold and Thrust Belt; WMR, Western Muller Ranges. Black dashed box indicates location of Fig. 1c. **(c)** Structural elements of the NWFTB, including the boundaries of the Greater Juha area which is the focus of this study. SRTM digital elevation model retrieved from USGS (2015). (For interpretation of the references to colour in this figure legend, the reader is referred to the web version of this article.)

related to the inversion of Early Mesozoic extensional architecture such as grabens and half-grabens (e.g., Hill, 1991; Buchanan and Warburton, 1996). Well control to the north and south of the 40 km wide, 100 km long Darai Plateau to the southwest of the KFTB (Fig. 1b), make it the best documented inversion structure. An abrupt northwards increase in sedimentary thickness from 2.2 km to 4.8 km across the frontal Darai Fault led Hill et al. (2010) to suggest it was originally a major, long-lived basin-bounding fault. Similar, largely uninverted examples of basement extension structures have also been recognised in reflection seismic to the foreland of the KFTB (Schofield, 2000; McConachie et al., 2000) and across the foreland region directly to the southwest of the NWFTB (Kawagle and Meyers, 1996; Bennett et al., 2000).

Regional northeast-southwest (arc-normal) lineaments cross-cutting the PFB have long been recognised in both geological and geophysical datasets, commonly from distinct lateral changes in structural style and/or sublinear arrangements of volcanics. The most prominent example is the approximately northeast-southwest trending Bosavi Lineament (Fig. 1b) (e.g., Hill, 1989; Smith, 1990; Hill et al., 2008). The Bosavi Lineament marks the transition from the KFTB oil province to the NWFTB gas province (e.g., Hill et al., 2008) and is characterised by a zone of structural disruption and an abundance of Plio-Pleistocene volcanoes. The structure appears to offset the KFTB and NWFTB dextrally (Fig. 1b) (Osborne, 1990), consistent with 3D numerical models that suggest arc-normal oriented weaknesses would be prone to oblique dextral, up-to-the-southeast offset during northeast-southwest compression (Gow et al., 2002).

Over the last few decades other regional-scale northeast-southwest trending lineaments have been recognised in the NGFB, often related to the emplacement of New Guinea's mineralised intrusive bodies (e.g., Davies, 1991; Corbett, 1994; Hill et al., 1996b; White et al., 2014). Lineaments recognised in West Papua have been linked to a similar northeast-southwest fabric within Proterozoic and Palaeozoic basement in northern Australia (Hill et al., 1996a,b). Recent work by White et al. (2014) using a range of geophysical data showed that the lineaments were most prominent in lower resolution data that imaged deeper in the crust (e.g., gravity and tomography), but were much less prevalent and much more complex than previously mapped. Arc-normal lineaments are most commonly related to the compressional reactivation of regional-scale lateral ramps, with local zones of dilatation linked to the intrusion of magmatic fluids (e.g., Hill, 1991; Hill et al., 2002).

In addition to regional-scale lineaments, local-scale arc-normal structures have also been identified throughout the PFB. In contrast to past studies, and to avoid ambiguity, we have chosen to

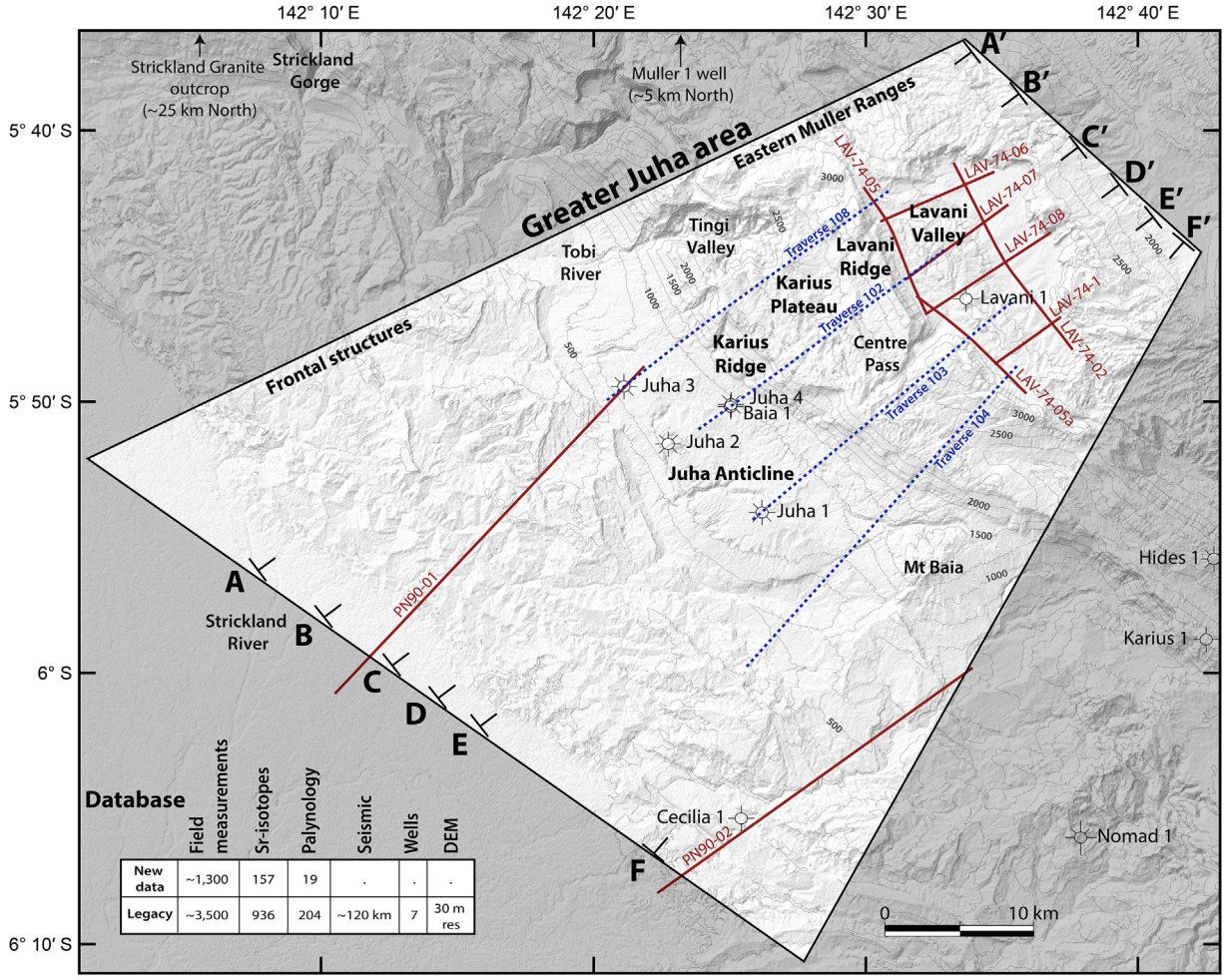

Fig. 3. Location of key localities and data sources within the Greater Juha area, including geological traverses (blue dash), available seismic lines (red), wells and cross-sections. Regional seismic lines PN-90-01 and PN-90-02, obtained in 1990 and reprocessed by Papuan Oil Search Ltd in 1996, have significantly improved our understanding of frontal structures. Lavani Valley seismic is of mostly poor quality and provides limited constraint. Geological traverses 102, 103, 104 and 108 have significantly increased the geological dataset across the Greater Juha area. SRTM digital elevation model retrieved from USGS (2015). (For interpretation of the references to colour in this figure legend, the reader is referred to the web version of this article.)

differentiate arc-normal lineaments observed in regional-scale datasets from arc-normal structures observed in local-scale datasets, noting that the relationship between regional arc-normal lineaments and arc-normal structures is largely unknown. Geological and geophysical data suggest steeply-dipping arc-normal structures are abundant across the PFB, most commonly recognised in basement structure and as tear faults within the sedimentary sequence (e.g., Hill, 1989; Hill et al., 2008; Craig and Warvakai, 2009).

2.2.1. The Greater Juha area

The structurally complex Greater Juha area is located in the frontal trend of the NWFTB where the dominant structural trend is northwest-southeast, connecting the WNW-ESE trends of the neighbouring KFTB and Western Fold and Thrust Belt (WFTB) (Fig. 1b). The overall deformational style of the Greater Juha area appears transitional between the low-relief, dominantly thin-skinned style of the KFTB (e.g., Hill et al., 2010) and the higher-relief, dominantly thick-skinned style of the WFTB (e.g., Eisenberg, 1996). The Greater Juha area is dominated by the Eastern Muller Ranges (EMR), which combined with the Western Muller Ranges (WMR) defines a large ~25 km wide uplifted region extending westward > 150 km to near the West Papua border (Fig. 1b). The rest of the Greater Juha area, as defined here, lies to the southwest of the EMR and comprises the ~15 km wide and ~25 km long Juha Anticline and much smaller <5 km wavelength structures including the Wai Asi and Cecilia Anticlines (Fig. 1c). The Pliocene-Pleistocene syn-tectonic sediments are well preserved across this frontal region where they are clearly co-planar with the underlying Darai Limestone. The extent and thickness of syn-tectonic sediments across the EMR prior to uplift and erosion is largely unconstrained.

2.2.2. Frontal structures

Despite considerable resource exploration throughout the frontal structures of the Greater Juha area, published geological and geophysical data are limited (e.g., Davies and Norvick, 1974; Craig and Warvakai, 2009; Hanani et al., 2016). The Cecilia Anticline demonstrates the forelandward extent of Cenozoic compression-related structures within the NWFTB. It has been tested by a single well, Cecilia 1 (Fig. 3), which intersected the Cecilia Thrust and an associated Darai Limestone repeat, subsequently failing to reach the Early Cretaceous Toro Sandstone reservoir target (Texaco, 1971). In contrast, the nearby Juha Anticline has a long history of exploration following the discovery of a significant gas column in the Juha 1 well (Fig. 3) (Niugini Gulf Oil, 1983). Good geological and geophysical data coverage reveals the doubly plunging nature and lobate morphology of the wide Juha Anticline (Fig. 1c), but the sub-

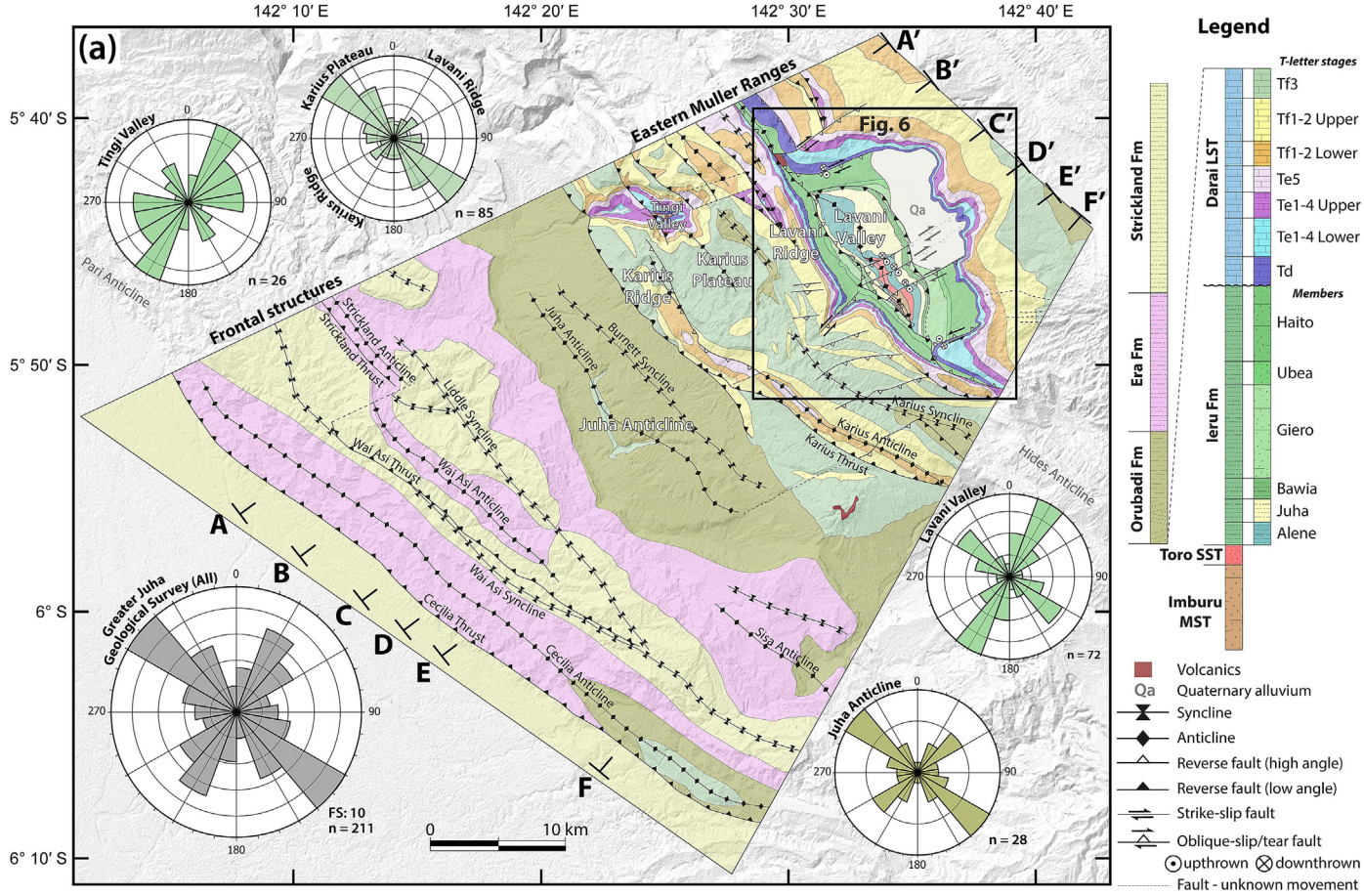

Fig. 4. (a) Geological map of the Greater Juha area including rose plots for fault and fracture strike across each subarea (see Fig. 3 for key localities and constraining data). The number of structural measurements (n) varies while the frequency scale (FS) is 5, except where otherwise stated. Representative strike and dip data, along with strontium isotope and palynological age constraints are included in Figs. S1 and S2 in the supplementary material. (b) Block diagram of quasi-3D model including the Greater Juha geological map and the six cross-sections constraining it. The Darai Limestone and Ieru Formation are sub-divided into T-letter stages and members, respectively (Fig. 3), in the cross-sections only where data permits. The vertical axis is in kilometres relative to mean sea level and is exaggerated by 1.5 times. (c) Segmented and total line length balance (LLB) shortening of the Darai Limestone horizon across the Greater Juha area. Shortening per segment is also included in (b). SRTM digital elevation model retrieved from USGS (2015).

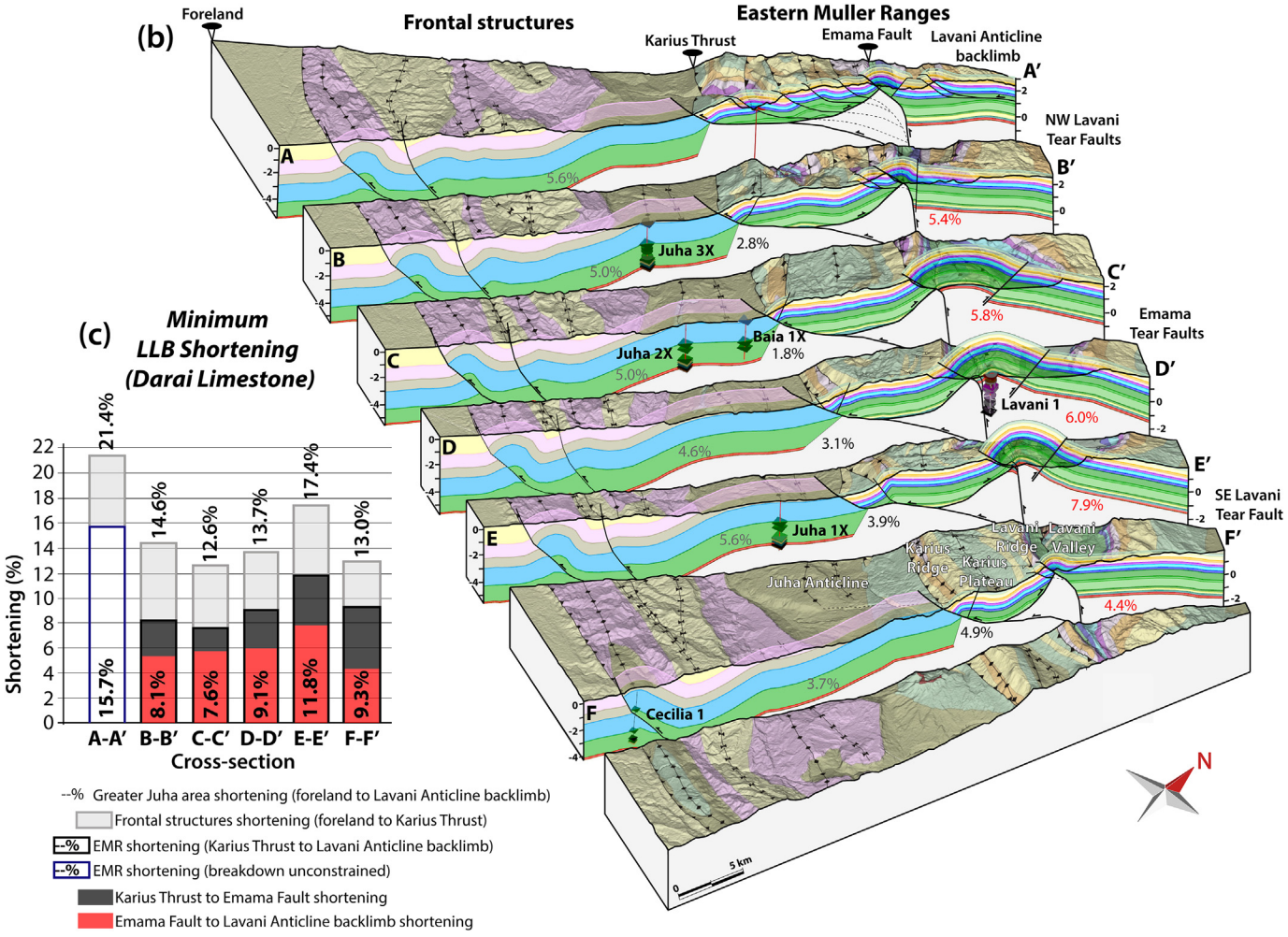

Fig. 4. (*continued*).

surface geometry of the structure remains poorly constrained. Both thin-skinned (e.g., Hobson, 1986; Hill, 1989) and thick-skinned (e.g., Hanani et al., 2016) structural models have been proposed.

Regional seismic data have significantly improved our understanding of frontal structures across the Greater Juha area (Fig. 3). Initial seismic interpretations by Craig and Warvakai (2009) identified a common sub-Darai Limestone detachment for the Cecilia, Wai Asi and Strickland Anticlines (see Fig. 4a for structure locations), but made no attempt to interpret the deep structure. Subsequent geophysical interpretation and kinematic modelling of the frontal structure by Hanani et al. (2016) suggests an inverted graben-bounding basement fault beneath the wide Juha Anticline that shallows into a detachment horizon within the Jurassic sedimentary sequence, before eventually connecting to the Cecilia and Wai Asi Anticlines through triangle zones within the Ieru Formation.

2.2.3. Eastern Muller Ranges

In the Greater Juha area, the EMR are dominated by the Lavani Anticline and its eroded core, the Lavani Valley (Fig. 1c). The Lavani Valley is unique, characterised by Late Jurassic to Late Cretaceous sediments cropping out >2.5 km above mean sea level (AMSL), suggesting uplift of >7 km relative to regional depth in the foreland. Several seismic lines and gravity data were acquired during the Lavani Valley Seismic Survey in 1974, prior to drilling of the dry Lavani 1 well (Amoco, 1982). The generally poor-quality seismic and gravity data revealed: (1) a large down-to-the-east basement-involved fault beneath the northwest end of Lavani Valley (LAV-74-06; Fig. 3); (2) a corresponding eastward decrease in gravity and (3) a positive gravity anomaly directly to the southwest of Lavani Valley (Bidstone et al., 1974). The Lavani 1 well spudded within Toro Sandstone near the centre of the Lavani Valley (Fig. 3) and initial interpretations of the well included a major northeast-dipping reverse or thrust fault at ~500 m repeating the Toro section (Amoco, 1982). However, improved palynological dating and stratigraphic understanding instead revealed a Koi-Iange repeat overlying a ~1.8 km thick sequence of syn-rift sediments of the Magobu Formation (Denison, 1990). Although thrust repeats may have contributed to the thickening of the Magobu Formation within the Lavani 1 well, they are unlikely to be solely responsible for the observed thickness. The dry Muller 1 well (Mobil, 1991), located to the northwest of the Greater Juha area (Fig. 1b) on the northwest plunging nose of the Lavani Anticline, is the only other well in the EMR. It spudded in basal Darai Limestone and drilled a conformable sequence intersecting the Toro Sandstone reservoir at 1.8 km downhole depth (Mobil, 1991).

The evolution of the EMR is poorly understood, with previous workers proposing a range of models to explain uplift, including: (1) basement-involved thrusting and inversion (e.g., Jenkins, 1974; Davies, 1983); (2) thin-skinned deformation (Hobson, 1986); (3) blind thrusting/passive-backthrusting (Buchanan and Warburton, 1996); (4) a basement-cored triangle zone (Hill, 1989) and (5)

igneous underplating (Buchanan and Warburton, 1996). Basement-involved thrusting is generally favoured due to the large positive gravity anomaly associated with the EMR (Bidstone et al., 1974) and the discovery of Triassic (222 ± 4 Ma from K-Ar; Page, 1976) granite basement in the Strickland Gorge in the core of the Muller Ranges (Fig. 1c) (Jenkins and White, 1970; White and Marfleet, 1973). Interestingly, in contrast to the ~1.8 km of syn-rift sediment intersected in the Lavani 1 well, syn-rift sediments are absent in the Strickland Gorge with the Strickland Granite directly overlain by ~1.2 km of Jurassic post-rift sediments (Niugini Gulf Oil, 1983).

3. Methods

We present new data and models for the structure of the Greater Juha area based on new field observations and reinterpretations of the legacy dataset. Field access to the remote Greater Juha area was facilitated through a program of data acquisition carried out along >100 km of traverses (Fig. 3) by Papuan Oil Search and ExxonMobil from 2013 to 2015. Very high rainfall upwards of 5000 mm per annum is common across the frontal mountain range of the PFB and has created a heavily karstified landform. Furthermore, steep terrain is prone to slumping and landslides that complicate the

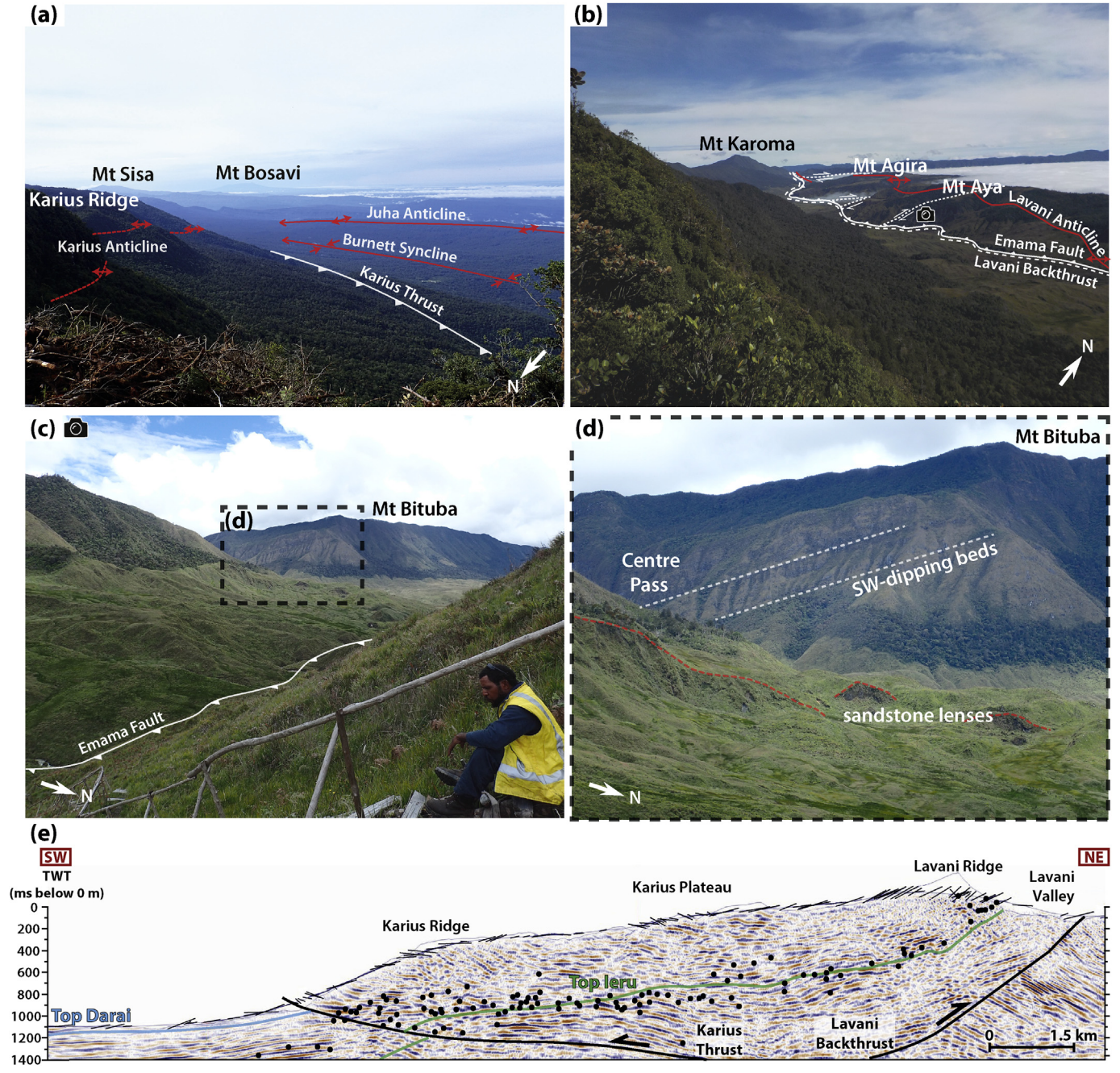

Fig. 5. (a) Foreland structures and the steep southwest-facing slope of Karius Ridge, looking southeast; (b) The major structural components and landform of the Lavani Valley from Lavani Ridge (Mt Uraka), looking northwest; (c) Centre Pass looking west from Mt Aya, with photo location marked in (b); (d) Centre Pass showing distinct southwest-dipping beds and northwest-southeast striking sandstone lenses within Ieru Formation at the base of Lavani Ridge, looking west; (e) Reflection seismic data across the EMR clearly show the shallowly northeast-dipping Karius Thrust and southwest-dipping Lavani Backthrust. Lines at surface are representative dip data and dots represent predicted Top-Ieru depth estimates based on strontium isotope ratios.

surface geology. Outcrop is limited (e.g., Fig. 5) due to thick vegetation, so geological data collection is challenging and the quality of field data can be variable.

Fieldwork included the description of lithologies, macrofossil assemblages and sedimentary structures (way-up) along with the measurement of ~1300 bedding, fault and fracture orientations (Fig. 3). In addition, 157 Darai Limestone samples were collected for petrographic, biostratigraphic and $^{87}Sr/^{86}Sr$ analysis. Strontium isotope ratios were related to larger benthic foraminiferal T-Letter stages widely used in the Indo-Pacific (e.g., Lunt and Allan, 2004) and calibrated to the geological timescale by strontium isotope stratigraphy through the Papuan Basin in ongoing CSIRO research (Fig. 2b) (e.g., Allan et al., 2000). An additional 19 Mesozoic clastic samples were dated palynologically. Data obtained during this study were added to legacy data to form a contemporary database across the Greater Juha area comprising ~4800 outcrops with both lithological descriptions and structural measurements (Fig. 3). Of these ~1300 outcrop samples were successfully dated using strontium isotope or palynological analyses (Fig. 3). Legacy datasets are available in reports to the Papua New Guinea Government.

We also make extensive use of NASA Shuttle Radar Topography Mission (SRTM) data, sampled at 1 arc-second, or ~30 m resolution (USGS, 2015). Midland Valley's Move software suite was used for cross-section and map construction. Cross-sections were constructed perpendicular to strike and spaced in order to best represent lateral structural variations and to optimally utilise the available data. Seismic data within the PFB are generally of poor to moderate quality, and thus the constraint on structure at depth is limited. In particular, data constraints drop off significantly below the top of the Ieru Formation and no attempt has been made to interpret structure at depths below the Ieru, except where well and seismic data exists such as across the frontal structures and within Lavani Valley (Fig. 3). Seismic lines recently acquired across the EMR (e.g. along Traverse 102, 103, 104, 108; Fig. 3) were not available at the time of this study, except for the shallow portion of Line 102.

The true stratigraphic thickness (TST) of Darai Limestone T-letter stages was estimated from traverse data and downhole strontium isotope ratio measurements in the Juha 1 well. TSTs were then combined with structural measurements to predict depth to the base of the Darai Limestone, following Hornafius and Denison (1993). TSTs for the Mesozoic sequence were estimated from a combination of traverse, well and seismic data, extrapolated from better constrained areas where necessary. For instance, substantial deformation and lack of outcrop within the Lavani Valley means that good quality data are limited and therefore TSTs are less constrained. In this case, TSTs from wells across the neighbouring Hides, Juha and Muller structures (Figs. 1b and 3) provided a valuable guide.

The process of integrating the geological map and cross-sections produced a quasi-3D model of much higher quality than a simple 2D geological map. The cross-sections ensure the map is geologically plausible in the third-dimension and enable sub-surface data such as reflection seismic and well-derived TSTs to be fully integrated.

4. Geological and structural observations

The Greater Juha area can be subdivided into five structural domains: the Juha Anticline, the Karius Ridge, the Karius Plateau, the Lavani Ridge and the Lavani Valley (Fig. 3). The structure of each domain is illustrated on the geological map and associated cross-sections in Fig. 4. Strontium isotope, palynological and representative structural data used to constrain the geological map and cross-sections are presented in Fig. S1 and Fig. S2 in the supplementary material.

4.1. Observed fault and fracture trends

Outcrop within the Greater Juha area is commonly faulted and fractured. More than 200 fault and fracture measurements reveal the overall dominance of northwest-southeast striking structures (Fig. 4a), consistent with the trend of the PFB in this region (Fig. 1b). The majority of these arc-parallel faults and fractures are bedding sub-parallel and most plausibly relate to flexural slip and glide mechanisms. There is also a strong northeast-southwest striking structural trend which is pervasive across the Greater Juha area, particularly in the Lavani and Tingi valleys where the Ieru Formation dominates surface outcrop (Fig. 4a). This arc-normal trend is also evident in the Orubadi Formation across the Juha Anticline, but is less prominent in the Darai Limestone across the Karius Ridge, Karius Plateau and Lavani Ridge (Fig. 4a). The reduced prominence in Darai Limestone may relate to its greater competence compared with mudstones and siltstones of the Ieru Formation. An alternate explanation is that arc-normal structures are more concealed within Darai Limestone outcrop due to denser vegetation and intense karstification.

The arc-normal structural trend can also be inferred on the SRTM digital elevation model (DEM) and identified in geological mapping (Fig. 4a), where it is expressed as: (1) discrete faults, such as observed in abundance across the southeastern end of the Karius Plateau; (2) through-going zones characterised by the termination or disruption of structures, such as at the northwest and southeast ends of the Juha and Lavani anticlines and/or; (3) geomorphic features, such as Centre Pass (Fig. 3). The prevalence of this arc-normal structural trend across multiple scales suggests it has played an important role in the structural evolution of the area.

4.2. Juha Anticline

The Juha Anticline mainly exposes Orubadi Formation (Fig. 4) the basal unit of which is an often cross-bedded, medium- to coarse-grained calcarenite, which appears to control the surface expression of the anticline such that the bedding orientation approximates the slope (Fig. 4b). Field and seismic data suggest that the Orubadi Formation calcarenite lies conformably on the uppermost Darai Limestone across the entire Juha Anticline. Faulting and fracturing along two dominant structural trends (Fig. 4a) forms a tessellated landform consisting of cliff-faces up to several metres high and crevices up to several metres deep. Fault movement sense could be determined for several faults, with reverse, strike-slip and oblique-slip faults identified, leading us to the inference that this characteristic landform could relate to local transpressional and transtensional interactions between discrete blocks. The calcarenite comprises highly competent beds so is a good analogue for structures in the underlying, very competent Darai Limestone where heavy karstification may mask structural trends.

4.3. Karius Ridge

The Karius Ridge is entirely composed of Darai Limestone and exhibits ~1 km of topographic relief from its base on the northeast-limb of the Juha Anticline to its crest on the Karius Plateau (Fig. 3). The dominant bedding dip appears to be sub-parallel to the southwest-facing slope, although common boulders and slumping across steep terrain in this area (Fig. 5a) make it difficult to obtain high-confidence data.

The most prominent structures along the length of Karius Ridge are the Karius Thrust and associated Karius Anticline (Figs. 4 and 5a). Strontium isotope analyses show the Karius Thrust

juxtaposes Tf3- to Te5-aged Darai Limestone in its hanging wall with younger Tf3-aged Darai Limestone and Orubadi Formation in its footwall, with the oldest hanging wall rocks cropping out in the hinge of the Karius Anticline (Fig. 4). Darai Limestone along Karius Ridge is anomalously deformed compared to the surrounding areas, with an increased abundance of arc-parallel faults and fractures and a stronger developed bedding-parallel stylolitic fabric. Over 30 southwest-facing cliffs, each up to several metres high, are particularly prominent on the southwest side of the ridge crest, inferred to relate to steeply northeast-dipping reverse faults (Fig. 5a). A stepped series of 10–20 northeast-facing cliffs, each up to 5 m high, dominate for ~1 km northeast from the crest of Karius Ridge, inferred to relate to steeply southwest-dipping backthrusts. These structures are here interpreted to be conjugate backthrusts in the hanging wall of the southwest-vergent Karius Thrust and appear to have contributed to the uplift and subsequent erosion of the Karius Anticline towards the northwest (Fig. 4). While a distinct fault was not observed in outcrop at the base of the Karius Ridge, seismic data clearly show the truncation of bedding at the base of the thrust sheet (Fig. 5e). The Karius Anticline appears to be tighter towards the southeast (Fig. 4b), which is consistent with observations of overturned bedding in the Karius 1 well and outcrop immediately to the southeast of the Greater Juha area (Fig. 3) (Johnstone and Emmett, 2000).

Darai Limestone cropping out on the southwest-facing slope of the Karius Ridge is significantly older than on the Karius Plateau (Fig. 4). This is a consistent geomorphic characteristic of frontal structures in the PFB (e.g., KFTB: Hill et al., 2008; Mananda Anticline: Keenan and Hill, 2015) that is in part related to increased rainfall and weathering along southwest-facing slopes.

4.4. Karius Plateau

Elevation along the Karius Plateau ranges from ~2–2.5 km AMSL along the crest of the Karius Ridge to ~3.2–3.6 km AMSL at the crest of Lavani Ridge (Fig. 3). The plateau broadens from ~4 km wide in the southeast to ~11 km wide in the northwest (c.f. cross-sections F-F′ and B-B' in Fig. 4b). Outcrop across the plateau is dominated by shallowly-dipping Darai Limestone that has suffered moderate to intense karstification, with abundant rillenkarren and sinkholes up to hundreds of metres across. While karstification makes it difficult to identify discrete structures, the landform is clearly intersected by sub-linear trending zones of cliffs up to 10 m high. These zones are interpreted to represent intersecting arc-parallel and arc-normal oriented structures that can also be readily observed cross-cutting Karius Plateau at the scale of the SRTM DEM (e.g., Fig. 6a).

Strontium isotope data show that Tf3- and TF1-2 (Upper)-aged Darai Limestone crops out across most of the Karius Plateau except where the Orubadi Formation was observed on Traverse 108 and to the southeast of Traverse 104 (Fig. 4). Interestingly, the basal Orubadi Formation calcarenite conformably overlying the Darai Limestone across the Juha Anticline is absent across the Karius Plateau on Traverse 108, suggesting that the Orubadi Formation may unconformably overlie the Darai Limestone. This is consistent with observations of a similar unconformity around the Muller 1 well to the northwest of the Greater Juha Area (Fig. 3) (Hornafius, 1993), suggesting an unconformity may extend across large portions of the EMR. Alternatively these observations could be explained by the strongly diachronous nature of the Orubadi Formation in this region (e.g., Thornton et al., 1996).

The shallow structure of the Karius Plateau is dominated by the Karius Syncline in the southeast passing into a series of southwest-verging thrusts in the northwest. The syncline tightens significantly towards the southeast in a similar style to the Karius Anticline (Fig. 4b). To the northwest of cross-section D-D′, the Karius Syncline is replaced by an almost continuous southwest bedding dip in cross-section C-C′ and by gentle folding in cross-section B-B'. Further northwest on cross-section A-A', smaller wavelength folds and small to moderate offset thrusts are inferred and strontium isotope ages show older Darai outcrops. This change in structural style is interpreted to be accommodated along an arc-normal oriented zone of tear faulting that extends from the northeast of Tingi Valley to Lavani Ridge (Fig. 4a).

The Tobi River has eroded up to 1 km into the Karius Plateau to the northwest of the Greater Juha area, forming the steep-sided Tingi Valley (Fig. 3). In places, the Tobi River has eroded through the entire Darai Limestone sequence (Fig. 4). A northeast-dipping thrust has tentatively been interpreted to cross-cut the Tingi Valley (Fig. 4), based on strontium isotope ratios and field observations. Intermediate volcanics of the Tingi Valley Igneous Complex, including both diorites and andesites, are abundant throughout the Tingi Valley with scattered hornblende-phyric andesitic boulders present as far away as Traverse 108 on the Karius Plateau. Field observations suggest that the volcanics have spread out at the Darai Limestone/Ieru Formation contact, possibly facilitated by cave systems observed near the base of the Darai Limestone within Tingi Valley.

4.5. Lavani Ridge

The regionally prominent Lavani Ridge is bound to the northeast and southwest by steep slopes and is characterised by a variable crest elevation of ~3.2 km AMSL on Traverse 103 at Mt Uraka, to ~3.6 km AMSL on Traverse 108 at Mt Karoma (Fig. 6a). Structural measurements and strontium isotope data across Lavani Ridge reveals a persistent shallow southwest bedding dip, as do observations from the cross-cutting Centre Pass (Fig. 5c and d).

The southwest-facing slope of Lavani Ridge mostly comprises Tf3- and Tf1-2 (Upper)-aged Darai Limestone (Figs. 4 and 6b). Older areas of Tf1-2 (Lower)- and Te5-aged Darai Limestone on the crest and southwest side of Lavani Ridge around cross-sections A-A′, B-B′ and F-F' are interpreted to result from uplift in the hanging wall of southwest-verging thrust faults (Figs. 4 and 6b). This is consistent with field observations from these areas including an order of magnitude increase in the intensity of faulting and fracturing when compared to Karius Plateau, and an increased abundance of southwest-facing cliffs up to 10 m high.

The northeast-facing slope of Lavani Ridge (Fig. 5c) comprises a ~1 km, mostly conformable sequence from Tf1-2 (Upper)-aged Darai Limestone to Ieru Formation (Figs. 4 and 6b). Palynological data indicate that sandstones, siltstones and mudstones cropping out near the base of Lavani Ridge, in Lavani Valley, belong to the Haito and Ubea Members of the Ieru Formation (Fig. 6b). Comparatively erosion-resistant, southwest-dipping sandstone beds form northwest-southeast striking ridges (Fig. 5d) that can be recognised in the high-resolution SRTM DEM and which demonstrate structural continuity (e.g., Fig. 6a).

Centre Pass is a prominent valley cross-cutting Lavani Ridge (Fig. 6a). The Emama River (Fig. 6a) appears to have once drained to the southwest through Centre Pass, but subsequent drainage reorganisation to the northeast and southeast of Lavani Valley has left Centre Pass virtually dry. The Tingi Valley has a similar geomorphic expression (Fig. 3) suggesting it is a potential modern analogue for fluvial incision of Centre Pass into Lavani Ridge. Interestingly, the strike of Centre Pass is similar to the prominent arc-normal structural trend recognised throughout the Greater Juha area (Fig. 4a). Sinistral offset of Lavani Ridge across Centre Pass is here interpreted to be related to tear faulting (Fig. 4).

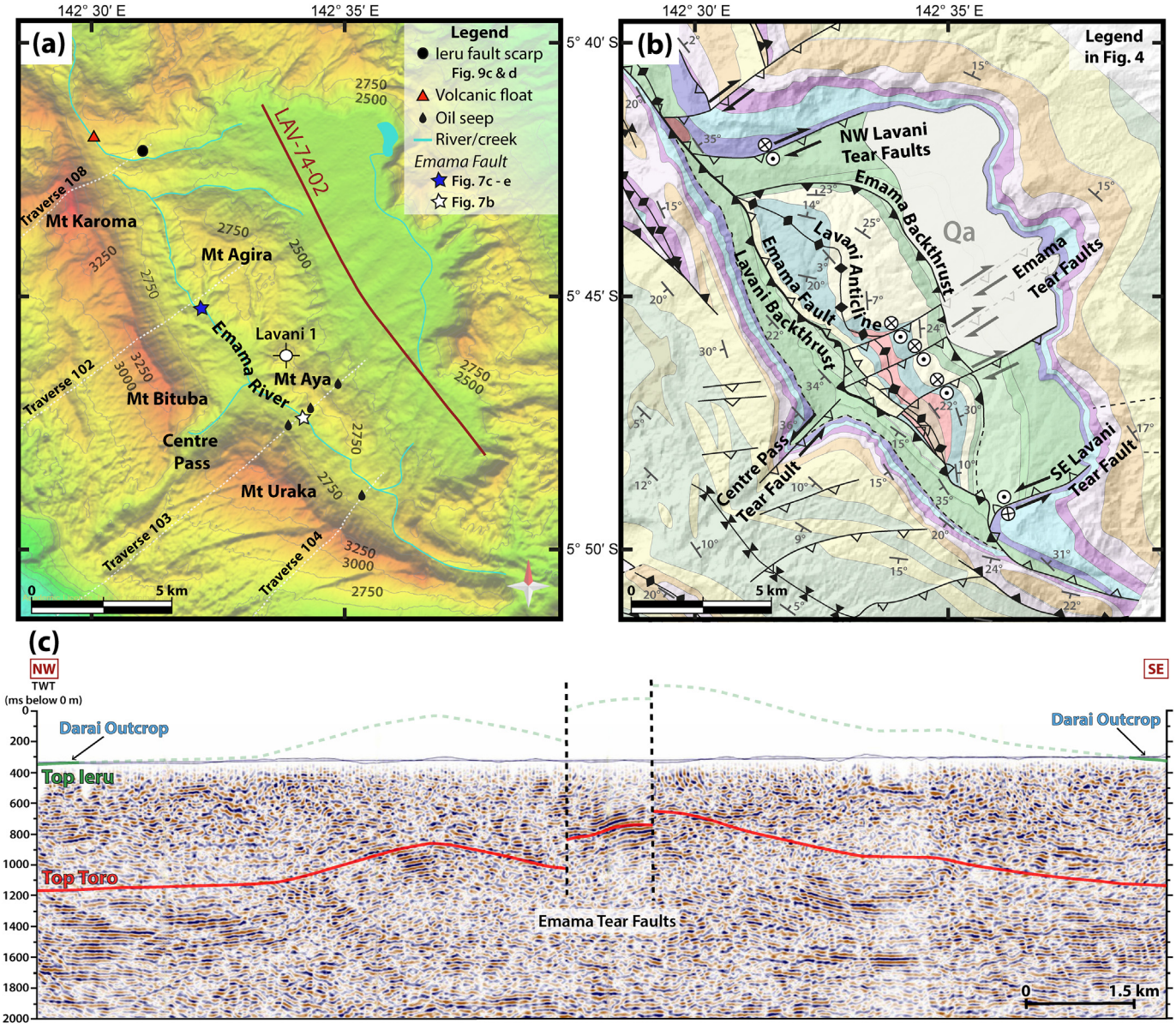

Fig. 6. (a) DEM of Lavani Valley and environs from SRTM dataset (USGS, 2015). Key geographic features and the location of geological traverses are indicated; (b) Detailed geological map of the Lavani Valley. Legend in Fig. 4. Note the dominant up-to-the-southeast offset on the NW Lavani Tear Faults, Emama Tear Faults and the series of faults cross-cutting the southwestern end of Karius Plateau. Variable topography combined with the vertical component of motion on the oblique-slip Emama Tear Faults masks the dextral sense of shear in map view. (c) LAV74-02 reflection seismic data along the length of Lavani Valley (location in (a) above) demonstrates up-to-the-southeast offset across the Emama Tear Faults, consistent with surface geological data (e.g., (b) above).

4.6. Lavani Valley

The ~10 km wide and ~15 km long Lavani Valley is located along the hinge of the regionally prominent Lavani Anticline (Figs. 5b and 6). The surface geology is dominated by mudstones, siltstones and minor sandstones of the Ieru Formation, contributing significantly to its distinct, comparatively gentle sloping and open landform (Figs. 5b and 6a). The valley is almost completely surrounded by steep slopes of mostly conformable Darai Limestone that dip away to the southwest and northeast on either side (Fig. 4b). The geology of the Lavani Valley offers significant insight into the structure of the regionally-significant Lavani Anticline as a whole and indeed the entire EMR.

Dense grassland vegetation means that outcrop within the Lavani Valley is largely limited to the Emama River (Fig. 6a), and consequently observations are available mostly along strike, with few cross-cutting traverses. Our work provides new observations of the dip structure across this area. Importantly, observations suggest that while faulting and fracturing is pervasive throughout the Lavani Valley, deformation is clearly more severe within major fault zones such as around the regionally significant Emama Fault (Figs. 4b and 6b and c.f. Fig. 7a and b).

4.6.1. Emama Fault

The Emama River is a consistent feature at the base of the southwest side of Mt Agira and Mt Aya (Fig. 6a). Major fault zones were observed at two localities around 6 km apart within the Emama River (Fig. 6a), suggesting the river approximately follows the trace of a major fault.

Morphologically, the fault appears sub-vertical on Traverse 102,

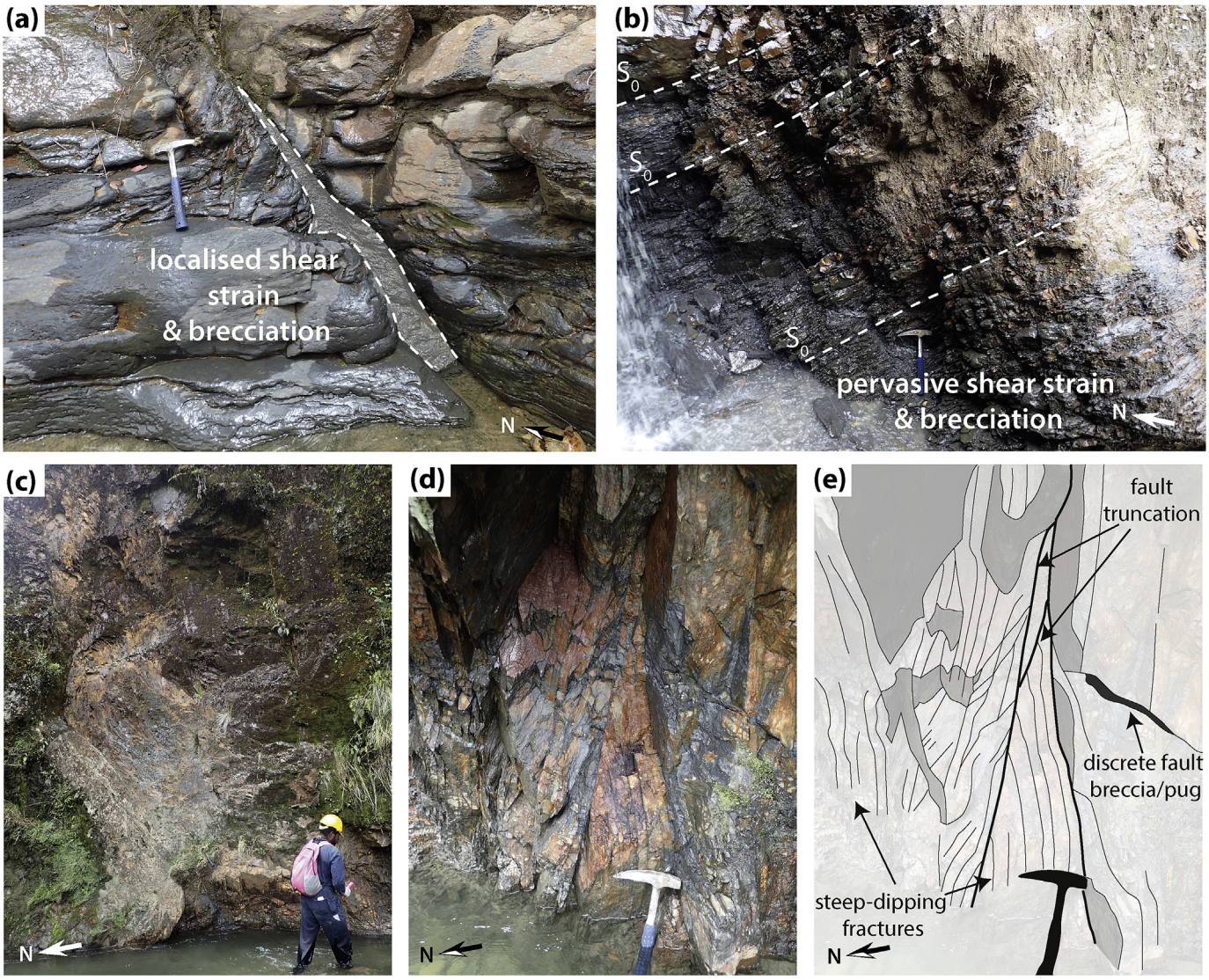

Fig. 7. Faulting within the Cretaceous Ieru Formation in Lavani Valley. (a) Abundant, widely distributed narrow/discrete (<1 m) faults and (b–e) wide fault zones (>10 m) with distributed shear strain. (b) Shows the Emama Fault on Traverse 103; (c), (d) and (e) show the Emama Fault along Traverse 102. Location of Emama Fault photos marked in Fig. 6a.

where it is expressed as a >10 m wide zone of steep, contorted bedding with localised fault gouge and brecciation (Fig. 7c–e). Around Traverse 103 the fault dips towards the northeast with fault rounded and striated fine-grained sandstone fragments within highly sheared mudstones (Fig. 7b) suggesting that the amount of movement accommodated within this zone is significant. Further, there is no evidence of a major fault along-strike in re-interpretations of the Lavani 1 well, suggesting the fault must become very steep down-dip (Fig. 4b, cross-section D-D'). This fault is here referred to as the Emama Fault (Fig. 6b), a steeply northeast-dipping reverse fault that uplifts Mt Agira and Mt Aya in its hanging wall and which may be largely responsible for the formation of the Lavani Anticline.

In the uplifted northeast side of the Emama Fault, the geological complexity appears to increase from Mt Agira in the northwest to Mt Aya in the southeast (Fig. 6). The surface geology of Mt Agira comprises a ~5 km wavelength anticline, with the Alene and Juha members of the lowermost Ieru Formation cropping out at its peak at ~2.8 km AMSL (Fig. 8a). Its forelimb is characterised by predominantly southwest-dipping beds (Fig. 8b and c) consistent with the adjacent Lavani Ridge (Fig. 5d).

In contrast, Mt Aya has an apparent wavelength of ~2.5 km, is noticeably more asymmetric (Fig. 6a) and Toro Sandstone crops out at its crest at ~2.8 km AMSL (Fig. 8d). Traverse 103 demonstrates persistent shallow to moderate northeast dip along the southwest-facing slope of Mt Aya (Fig. 8e and f), suggesting the forelimb of the Lavani Anticline is mostly absent (Fig. 4b, cross-section E-E'). There is an accompanying increase in deformation intensity in this area, including widespread bedding sub-parallel shear strain, particularly evident in fine-grained lithologies (e.g., Fig. 7b). Traverse 103 also revealed a ~120 m thick sequence of fine- to coarse-grained sandstones located directly above intensely deformed Alene Member in the hanging wall of the Emama Fault. Earliest Cretaceous (Berriasian) palynological ages indicate that this sequence is the Toro Sandstone. Interestingly, previously unidentified sheared mudstone and siltstone directly overlying the sand-dominated sequence are of Late Jurassic (Tithonian) age, suggesting Imburu Mudstone directly overlies Toro Sandstone in this area. If correct, these are the oldest outcropping rocks in the Greater Juha area (Fig. 6b). Northeast-dipping Toro Sandstone crops out again at the

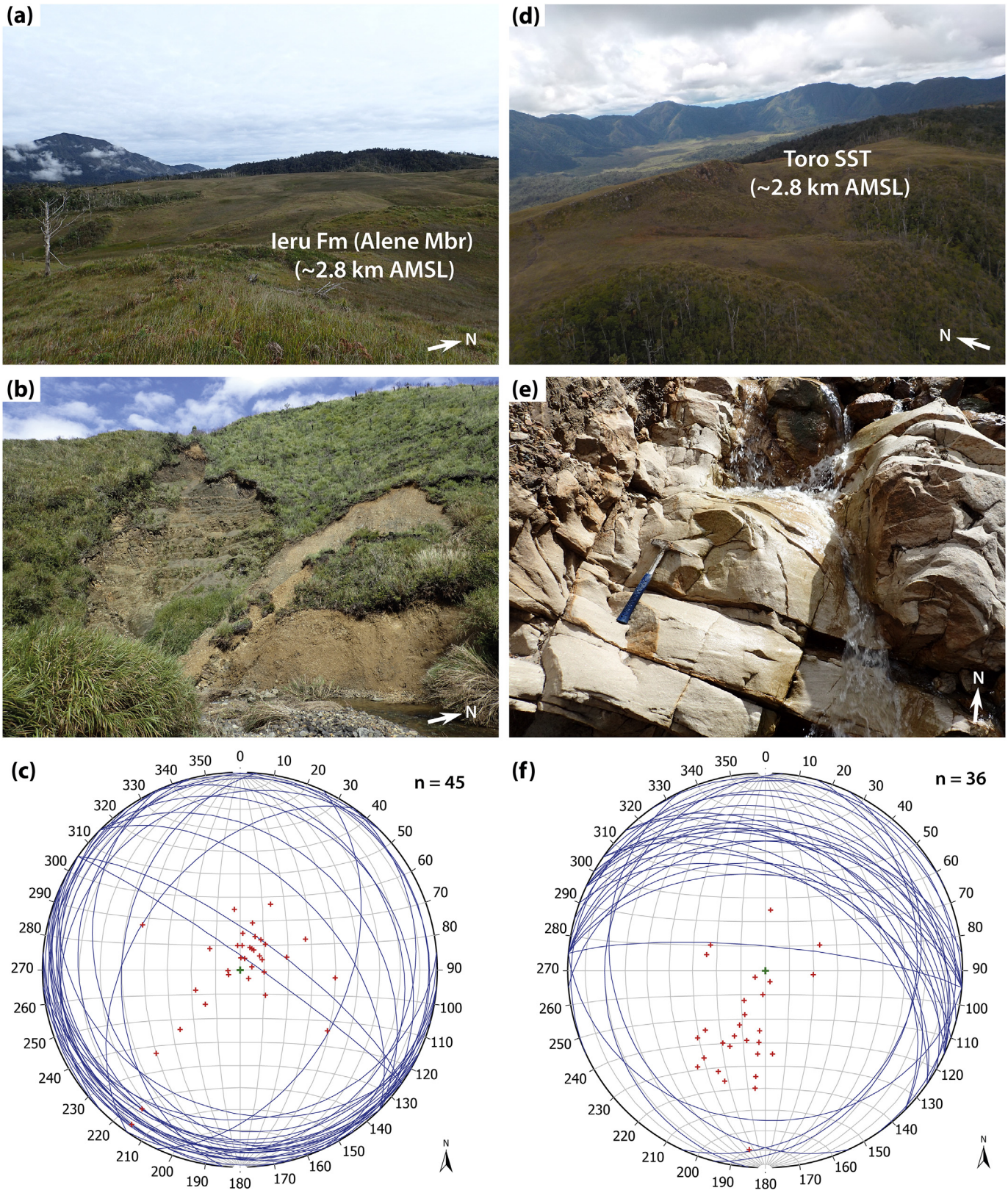

Fig. 8. Field photos and Schmidt stereonets (n = number of measurements) showing lateral geological variation within Lavani Valley. Mt Agira (Traverse 102) is associated with; (a) a relatively subdued landform; (b) Ieru Formation outcrop and (b & c) a southwest bedding dip. In contrast, Mt Aya (Traverse 103) is associated with (d) a steeper landform; (e) older outcrop, including Toro Sandstone and (e) & (f) a northeast bedding dip.

crest of Mt Aya (Fig. 8d) as originally reported by Bidstone et al. (1974). Several low to moderate confidence way-up indicators (e.g., graded-bedding, cross-bedding) along the length of Traverse 103 suggest that the sedimentary sequence is the right way up, however we are hesitant to completely rule out the possibility of an overturned limb.

Thus, the geometrically complex Emama Fault is a regionally significant structure that appears to be largely responsible for uplifting the Lavani Anticline in its hanging wall. Further, the intersection of thick syn-rift sediments nearly 2 km AMSL in the Lavani 1 well suggests the Emama Fault is connected to an inversion structure at depth; a decrease in Bouguer gravity from Lavani Ridge into Lavani Valley (Bidstone et al., 1974) suggests that, despite inversion, basement remains deeper in the hanging wall of the Emama Fault.

In summary, geological field data from within Lavani Valley reveal the structural complexity of the Emama Fault and Lavani Anticline. Outcropping rocks become older towards the southeast of Lavani Valley (Fig. 6b), suggesting increased displacement and hanging wall uplift along the Emama Fault towards the southeast. The southwest-facing slope of Mt Aya provides important insight into the subsurface structure of the Lavani Valley. Here, thrusted repeats of Ieru Formation, Toro Sandstone and Imburu Mudstone are interpreted as stacked horses with the bounding faults merging into a foreland-vergent roof thrust within the incompetent Ieru Formation (Fig. 4b, cross-section E-E'). This roof thrust and the overlying hangingwall rocks have since eroded away adjacent to Mt Aya. It is unclear whether this structural style extends along strike to beneath Ieru Formation cropping out over Mt Agira (Fig. 6b), but if so the roof thrust must lie just beneath the surface in the Alene Member, suggesting this is a prominent detachment layer. Alternatively, the structural style may change at a tear fault.

4.6.2. Emama Backthrust

Field data constraints across Mt Agira combined with the LAV74-02 seismic line to the northeast (Fig. 6a and c) define an abrupt transition from lower to upper Ieru Formation members around the northern flank of Mt Agira (Fig. 6b). In the absence of the steep bedding dips, the Emama Backthrust has been interpreted to explain this transition. Where it wraps around the northwestern flank of Mt Agira, the Emama Backthrust juxtaposes Bawia Member of the lowermost Ieru Formation with Haito member of the uppermost Ieru Formation (Fig. 6b). The significance of the Emama Backthrust decreases towards the southeast where seismic line LAV74-02 suggests older Ieru Formation crops out in its footwall (Fig. 6c). Moreover, it is plausible that uplift in the hanging wall of the Emama Backthrust has had a geomorphic control on the extent of Quaternary alluvium in the north of Lavani Valley (Fig. 6b).

4.6.3. Lavani Backthrust

Lavani Ridge appears to be located within the footwall of the Emama Fault, but is nevertheless associated with elevations >3.2 km AMSL along its length, making it the highest topographic feature in the Greater Juha area. Furthermore the steep northeast-facing slope appears to be unique regionally within the NWFTB, where the vast majority of steep slopes are southwest-facing (Fig. 1c). We interpret these characteristics to result from uplift along a significant backthrust within the Ieru Formation that originates from beneath Karius Ridge (Fig. 4b). This backthrust is imaged on seismic data where it truncates bedding beneath Lavani Ridge (Fig. 5e). Exactly where the backthrust intersects the surface within Lavani Valley is less clear, but strontium and palynological data from the northeast-facing slope of Lavani Ridge suggest a largely conformable sequence, such that the Lavani Backthrust may intersect the surface at approximately the same location as the Emama Fault (Figs. 4b, 5b and 6b). This makes it difficult to constrain the relative influence of the Emama Fault and Lavani Backthrust. Thickness variations within the lower Td Darai Limestone, particularly to the southeast of Lavani Valley, suggest the Lavani Backthrust could plausibly have a splay near the Darai Limestone/Ieru Formation contact (Fig. 6b).

4.6.4. Arc-normal structures

Throughout Lavani Valley, arc-normal faults and fractures are pervasive (e.g., Fig. 9a and b) and may even be more abundant than arc-parallel structures (Fig. 4a). Interestingly, arc-parallel structures, typically bedding (S_0) parallel, show evidence of both brittle and semi-ductile (e.g., Fig. 9b) deformation. In contrast, cross-cutting arc-normal structures appear to have formed exclusively from brittle processes (Fig. 9a and b) and often displace arc-parallel structures.

Additionally, a small southeast-facing fault scarp (Fig. 9c and d) was observed within the Ieru Formation near the end of Traverse 108 (Fig. 6a). Such an observation is abnormal within the usually very fast weathering mudstones and siltstones of the Ieru Formation, suggesting that arc-normal faulting may still be active, at least within the Lavani Valley. Slickenfibres and striations confirm a northeast-southwest striking fault plane with at least a component of strike-slip movement (Fig. 9c and d). Thus, the scarp is likely to relate to a restraining bend/transpressional zone along a strike-slip or tear fault. Given its proximity to the abrupt northwest termination of the Lavani Valley, it seems plausible that this scarp is related to a larger zone of significant northeast-southwest striking faults, here collectively defined as the NW Lavani Tear Faults (Fig. 6b).

Other prominent northeast-southwest striking structures can be identified at the scale of Lavani Valley. The most significant of these appear to be located at the southeast termination of Lavani Valley (SE Lavani Tear Fault) and in a zone through the centre of Lavani Valley (Emama Tear Faults) (Fig. 6b). The tear faults bounding either end of the Lavani Valley are recognised by the vertical juxtaposition of older than expected Ieru Formation members with the Darai Limestone (Fig. 6b). The Emama Tear Faults cutting through the centre of the valley are defined by lateral changes in landform, along with surface and subsurface geology (Fig. 6). Reflection seismic line LAV74-02 demonstrates a component of up-to-the-southeast offset across the Emama Tear Faults (Fig. 6c), consistent with surface geological observations (e.g., Fig. 6b). Interestingly, the horizontal component of displacement along the Emama Tear Faults appears to be dextral between Mt Agira and Mt Aya and sinistral through the Lavani Ridge (Fig. 6b). The Emama Fault and Lavani Backthrust are located between this apparent change in movement sense, suggesting they may be related.

4.6.5. Summary

New observations presented here significantly improve our understanding of the structure of Lavani Valley. First, the Emama Fault is a geometrically complex, regionally significant structure that is largely responsible for uplifting the Lavani Anticline. Thick syn-rift sediments in the hanging wall suggest the Emama Fault is connected to an inversion structure at depth; a decrease in Bouguer gravity from Lavani Ridge into Lavani Valley (Bidstone et al., 1974) suggests that, despite inversion, basement remains deeper in the hanging wall of the Emama Fault. The amplitude and wavelength of the Lavani Anticline decreases outwards from the northwest and southeast ends of Lavani Valley (Fig. 4b, cross-section A-A′ and F-F′); suggesting that the Emama Fault may be associated with less displacement in these areas (at least at depth). Interestingly, outcropping rocks become older from the northwest to southeast of

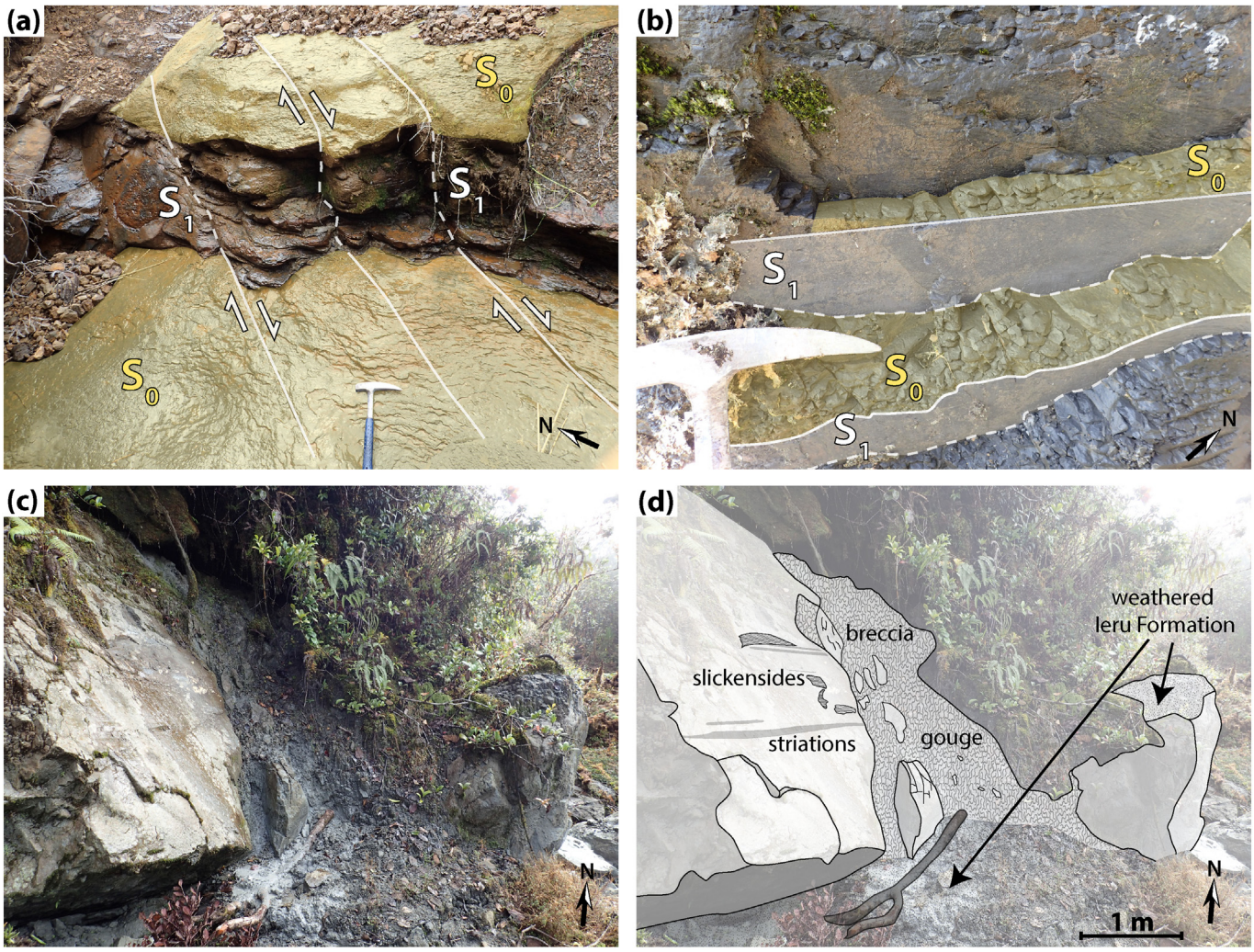

Fig. 9. Examples of outcrop scale arc-normal structures (S_1) in Lavani Valley including (a) northeast-southwest striking faults, predominantly associated with a component of dextral offset; (b) abundant northeast-southwest striking fractures across which offset is indeterminate or absent. Note the apparent change from wavy, semi-ductile, bedding parallel deformation (S_0) to the much more sharply defined brittle deformation (S_1). (c & d) a fault scarp within fast weathering Ieru Formation suggesting very recent to active strike-slip faulting (see Fig. 6a for location).

Lavani Valley (Fig. 6b) implying increased displacement and hanging wall uplift along the Emama Fault towards the southeast (Fig. 4b, c.f. cross-sections B-B′ and E-E').

Forty kilometres along strike to the northwest, basement crops out at ~500 m AMSL in the Strickland Gorge yet it was not encountered in the Lavani 1 well that extends ~200 m below mean sea level, implying basement deepens towards the southeast. This is consistent with eastward decreasing Bouguer gravity and a large down-to-the-east basement fault recognised in seismic data within Lavani Valley (Bidstone et al., 1974).

Together these observations clearly show that areas with the deepest basement and thickest syn-rift sediments have undergone the most significant uplift during basin inversion. Thus, pre-compression margin architecture was complex and appears to have had a significant influence on evolution. Moreover, arc-normal structures appear to be closely associated with lateral changes in geology along the Lavani Valley and therefore may represent zones of tear faulting - some of which remain active.

4.7. Shortening analysis

Shortening calculations are a powerful method of quantitatively assessing lateral geological variation and can thus assist in identifying accommodating structures such as tear faults. Here, a line length balancing (LLB) technique was used to estimate shortening of the well-constrained Darai Limestone horizon in each of the cross-sections.

Minimum estimates for Darai Limestone shortening across the entire Greater Juha area vary from 12.6 to 21.4% (Fig. 4c), with the greatest shortening correlating with increased structural complexity along cross-section A-A' (Fig. 4a and b). Here, shortening analyses are broken down into subareas (Fig. 4c) to investigate potential relationships between lateral shortening variations and arc-normal structures observed across the Greater Juha area (e.g., Section 4.6.4). It is important to note that the complexity of the Darai Limestone in the Lavani Anticline in cross-section A-A′ highlights the potential for complex structure within the hinge of the Lavani Anticline where the Darai Limestone has been eroded in Lavani Valley. Here, we present the simplest structural interpretation for eroded portions of the crest of the Lavani Anticline (e.g., Fig. 4b, C-C′ to E-E') so that shortening estimates are likely to be minima.

Along the EMR (excluding cross-section A-A′), minimum shortening of the Darai Limestone from the Karius Thrust to the

backlimb of the Lavani Anticline varies from 7.6 to 11.8% (Fig. 4c). Cross-section E-E′ was associated with the greatest shortening (11.8%), with shortening generally decreasing in sections to both the northwest and southeast. Cross-section A-A' has anomalously high shortening (15.7%) but with additional surface geological constraints meaning that this represents a maximum rather than minimum shortening estimate. However, comparably high shortening may at least partially be attributed to an interpreted increase in structural complexity (Fig. 4a and b).

Shortening estimates from the Emama Fault to the backlimb of the Lavani Anticline show a similar trend to the Greater Juha area and EMR shortening estimates (Fig. 4c). Importantly, cross-section E-E′ has minimum shortening Darai Limestone interpreted above the eroded Lavani Anticline, yet has still undergone at least 700 m more shortening than cross-section F-F′, which has an almost complete Darai limestone section. Furthermore, E-E′ has ~450 m more shortening than cross-section C-C'. We suggest that lateral shortening variations of this magnitude may be at least partially accommodated along the SE Lavani Tear Fault and Emama Tear Faults respectively (Figs. 4b and 6b). Shortening variation is much less significant between cross-sections C-C′ and B-B' (<100 m) and thus does not offer convincing support for the presence of the NW Lavani Tear Faults, interpreted based on field observations and geological constraints (Fig. 4a).

Shortening of the Darai Limestone from the Karius Thrust to the Emama Fault appears much lower, varying from 1.8 to 4.9%. With the exception of cross-section A-A′, there is a general increased shortening trend from northwest to southeast, consistent with increased tightening of the Karius Syncline (Fig. 4a and b). Interestingly, the presence of the Centre Pass Tear Fault is supported by a difference in shortening between cross-sections C-C' (1.8%) and E-E' (3.9%) that equates to at least 300 m of lateral shortening variation accommodated along this structure.

5. Structural evolution of the Greater Juha area

There is significant evidence for extension and rifting along the New Guinea margin in the early-Mesozoic, including in the foreland directly adjacent to the Greater Juha area. Observations outlined here suggest this variable pre-existing rift architecture almost certainly underlies the Greater Juha area and has had significant influence on the evolution of structural styles during Cenozoic compression of the New Guinea margin.

There is substantial geological and geophysical evidence suggesting that the Juha and Lavani anticlines formed above partially inverted grabens. Firstly, these structures can be linked through substantial similarities in orientation and morphology (Fig. 1c), with their large wavelengths, asymmetric limbs and lobate morphologies characteristic of inversion structures (e.g., McClay, 1995; Bonini et al., 2012). Geophysical data across the Lavani Valley (Bidstone et al., 1974) and the thick Triassic synrift sequence intersected at ~1.9 km AMSL in the Lavani 1 well (>7 km above its foreland regional) presents a strong argument for the partial inversion of a graben beneath Lavani Valley. In fact, in order to sufficiently uplift the Lavani Anticline while still honouring geophysical observations of only partial inversion (i.e. basement hanging wall remains lower than basement footwall), the Lavani half-graben is likely originally to have been very deep, containing more than 7 km of syn-rift sediments (e.g., c.f. Fig. 10a and e).

Evidence from the Juha Anticline is less convincing but limited seismic and gravity data suggest it is also underlain by a deep graben (e.g., Hanani et al., 2016). Therefore the pre-compression architecture of the Greater Juha area may have included a set of listric northeast-dipping basement extensional faults and rotated basement hanging wall blocks responsible for the formation of the Juha and Lavani half-grabens (Fig. 10a).

Compression associated with continental collision along the New Guinea margin was originally accommodated within the Greater Juha area by the inversion of the normal-fault bounding the Lavani half-graben. The resulting steep Lavani inversion fault intersected the surface as the Emama Fault and the less significant Emama Backthrust, uplifting the Lavani Anticline (Fig. 10b). This occurred out-of-sequence early in the evolution of the NWFTB, as indicated by the relatively undeformed backlimb of the Lavani Anticline (Figs. 1 and 4a and b).

We suggest that during the evolution of the Lavani Anticline, the Lavani inversion fault shallowed into the incompetent Mesozoic sedimentary sequence beneath Lavani Ridge and, to a lesser extent, Karius Plateau. A single triangle zone—or more plausibly multiple triangle zones—formed within the Mesozoic sequence over this time, connected to a passive roof thrust, the Lavani Backthrust, within the Ieru Formation (Fig. 10c). This style of deformation relates to competence variations within the stratigraphic column, with the competent Darai Limestone much more resistant to shortening than the less competent underlying Mesozoic sequence. The forelandward propagating triangle zone(s) uplifted the Lavani Ridge, at least temporarily forming a frontal monocline (Fig. 10c) – a common characteristic of triangle zone-related deformation (e.g., Cooper, 1996 and examples within).

The Karius Thrust and associated Karius Anticline are here attributed to the most recent pulse of movement along the Lavani inversion fault (Fig. 10d). The now dry Centre Pass valley (see Section 4.5) provides considerable insight into the relative temporal evolution of this area of the EMR, with incision of the valley into the Lavani Ridge pre-dating uplift along Karius Ridge. Note the similarities between the structure of the Lavani Anticline in Fig. 10d compared to the present structure of the Juha Anticline on Fig. 10e (Hanani et al., 2016). This is consistent with the southwest propagation of the same structural style.

Despite their morphological similarities, the Juha Anticline has experienced significantly less uplift than the Lavani Anticline (Fig. 10e). One obvious difference between the two structures is the absence of an emergent frontal fault on the Juha Anticline (Fig. 4a and b). This characteristic suggests the Juha inversion fault shallows into the Mesozoic sedimentary sequence before connecting with forelandward structures (Fig. 10e), as suggested by Hanani et al. (2016). Important implications of this relationship are that displacement along the Juha inversion fault is restricted by the limited amount of displacement observed along structures towards the foreland (Fig. 4b).

5.1. 3D structural evolution of the eastern Muller Ranges

Observations from geological and geophysical data across Mt Aya in the Lavani Valley form a crucial foundation for our understanding of the 3D structural evolution of the EMR. In particular, the intersection of thick syn-rift sediments in the Lavani 1 well suggests the area was a regionally significant depocentre during Early Mesozoic rifting. But at the same time these sediments have been uplifted such that Jurassic strata crop out at the crest of Mt Aya indicating it has experienced the greatest uplift in the EMR and possibly in the entire PFB. Thus, there is a strong correlation between the magnitude of extension along the half-graben bounding Lavani normal fault and subsequent inversion along the Lavani inversion fault, a relationship also recently recognised within the Taranaki Basin in New Zealand (Reilly et al., 2016). The following model for the evolution of the EMR fits well with this type of inversion fault behaviour.

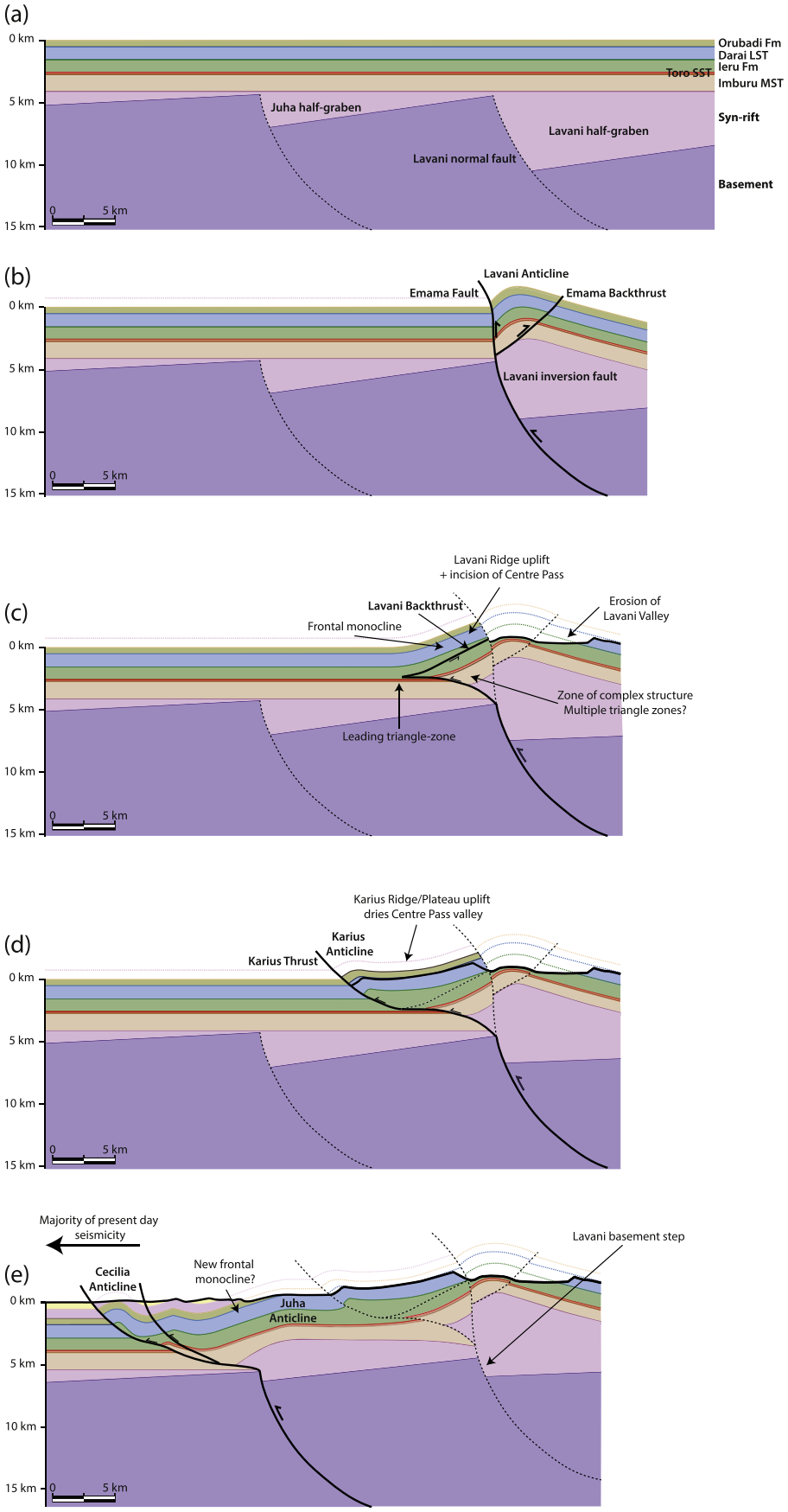

Fig. 10. Proposed schematic structural evolution of the Greater Juha area: (a) prior to compression; (b) during initial inversion and reverse displacement along the Lavani inversion fault, Emama Fault and Emama Backthrust; (c) during displacement along the Lavani Backthrust; (d) during displacement along the Karius Thrust and (e) during displacement along the Juha inversion.

5.1.1. Early Mesozoic extension

Northeast-southwest to NNE-SSW extension of the Papua New Guinea margin in the Early Mesozoic (e.g., Home et al., 1990) was associated with the formation of the regionally extensive northwest-southeast striking Lavani normal fault beneath the present day EMR (Fig. 11a). Over the course of the extensional evolution, a regional-scale, southeast-dipping relay ramp formed from at least as far northeast as the Muller 1 well (Fig. 1b) to the southeast-end of the present day Lavani Valley. This ramp may have formed to transfer extension between the Lavani normal fault beneath the EMR and another major basin-bounding normal fault to the north which continues into the WMR or Om Metamorphics (Figs. 1b and 11a). Syn-rift sediments accumulated on this regional relay ramp during its evolution, leading to thicker sediments towards the base of the ramp around the present day Lavani Valley.

Displacement along the Lavani normal fault was greatest towards its centre beneath the present day Lavani Valley, and decreased towards the southeast and northeast ends, thus approximating a commonly observed normal fault displacement-distance relationship (e.g., Muraoka and Kamata, 1983; Peacock and Sanderson, 1991; Gupta and Scholz, 2000; Frankowicz and McClay, 2010), but with an apparent level of asymmetry resulting from displacement decreasing more abruptly towards the southeast than the northwest (Fig. 11b). Here, this asymmetry is interpreted to have been accommodated along a number of cross-cutting, oblique-slip normal faults that breached the footwall block including the southeast-dipping relay ramp (Fig. 11b). Alternatively, the development of secondary oblique to cross-cutting structures could plausibly relate to an evolving extension direction on the New Guinea margin, in a style analogous to the nearby Bonaparte Basin in North West Australia (Frankowicz and McClay, 2010). A smaller relay ramp may have also formed at the southeast end of the present day Lavani Valley, but if so, was abruptly breached to accommodate a more rapid transition to higher displacement along the Lavani normal fault to the northwest (Fig. 11a and b). This scenario would have left a transfer fault that during subsequent extension may have connected the Lavani normal fault to another normal fault towards the east (Fig. 11a).

Relay ramps form as a means of transferring extension between overlapping normal faults and breaching is common (e.g., Hus et al., 2005; Fossen and Rotevatn, 2016). The example presented here differs in that multiple normal faults cross-cut the southeast-dipping relay ramp, representing a distributed zone of breaching rather than a single breach (Fig. 11a and b). Outcrop-scale evidence from better constrained extensional systems suggest that breached ramps are commonly complex, often involving multiple cross-cutting faults (Soliva and Benedicto, 2004). Pre-existing weaknesses are a likely influence on the evolution of multiple cross-cutting faults, as observed in Canyonlands National Park, Utah, where cross-cutting normal faults have formed along relay ramp-intersecting joint sets (Trudgill and Cartwright, 1994; Fossen and Rotevatn, 2016).

5.1.2. Cenozoic compression

Northeast-southwest compression associated with the formation of the PFB reached the Muller Ranges around the Late Miocene (Hill and Gleadow, 1989). The regional extent and large displacement of the Lavani normal fault made it particularly preconditioned for subsequent inversion (as per Eisenstadt and Withjack, 1995; Kelly et al., 1999; Panien et al., 2005; Reilly et al., 2016). However, despite significant inversion and hangingwall uplift along the Lavani inversion fault, it remains lower than the footwall beneath Lavani Ridge and Karius Plateau in the present day (Figs. 10e and 11d) (e.g., Bidstone et al., 1974).

Reverse displacement along the Lavani inversion fault was heterogeneously distributed with a strong correlation with its original extensional displacement (c.f. Fig. 11b and d). Similar to the rifting phase, inversion-related displacement differences were accommodated along the length of the relay ramp by inversion of oblique-slip cross-structures that subsequently dispersed into the sedimentary sequence forming the distributed regions of tear faulting observed in Lavani Valley (Fig. 11d). These zones are therefore characterised by the opposite movement sense to the original extension-related basement cross-structures (c.f. Fig. 11b and c). The greatest reverse displacement along the Lavani inversion fault and associated Emama Fault occurred around Mt Aya, where the sedimentary sequence was uplifted more than 7 km above regional. The great depth of basement beneath Mt Aya prior to compression (Fig. 11a and b) was crucially important in allowing such significant uplift without an associated present-day gravity high.

During the evolution of the EMR, the Lavani inversion fault shallowed to form triangle-zones beneath Lavani Ridge and Karius Plateau, with shortening of the Mesozoic sedimentary sequence accommodated along the Lavani Backthrust (Figs. 10c and 11d). Continued heterogeneous displacement along the Lavani inversion fault was then transferred to the surface largely along the Lavani Backthrust, causing increased northeast-directed thrusting of the Lavani Ridge into the southeast-end of Lavani Valley, driving sinistral offset at the Centre Pass Tear Fault (Fig. 11d). This model for the evolution of Centre Pass also accounts for opposing movement senses observed along the seemingly continuous Emama Tear Faults and Centre Pass Tear Fault; that is, each formed from a consistent shortening regime, but relate to structures with opposing vergence. During the final stages in the evolution of the EMR, the Karius Thrust uplifted Karius Ridge creating the Karius Anticline and Karius Syncline across Karius Plateau (Figs. 10d and 11d).

6. Discussion

6.1. Controls on structural style

The well-constrained Darai Limestone shows very low shortening of 12.6–21.4% across the Greater Juha area (see Section 4.7), which is unusual given the high magnitude of uplift across the EMR. In comparison, the much less elevated KFTB (Fig. 1b) is characterised by > 40% shortening (Hill, 1991). Triangle zone-related deformation is often invoked to explain large, internally complex mountain front structures characterised by only minor near-surface shortening (e.g., Suppe, 1980; Jones, 1996) and this model is consistent with structures observed within the leading-edge of the PFB including (from southeast to northwest) the Puri Anticline (Medd, 1996), Cecilia Anticline (Hanani et al., 2016) and P'nyang Anticline (Eisenberg, 1996). In the elevated EMR, the regionally-prominent Lavani Backthrust provides a mechanism to transfer shortening within the incompetent Early Mesozoic sequence through the competent Darai Limestone. Through time, as the Lavani Anticline was initially uplifted and eroded to form the Lavani Valley, this discontinuity within the Darai Limestone provided an easy pathway for shortening to reach the surface without having to be accommodated within thick competent Darai Limestone towards the foreland. Geological and geomorphic evidence suggests that the significance of the Lavani Backthrust decreases towards the northwest of the EMR, limiting the amount of shortening it can accommodate. In this area there is a recognisable change in structural style including increased structural complexity, more distributed and greater overall shortening within the Darai Limestone (e.g., cross-section, A-A′) meaning there are more structures likely to account for uplift of the EMR.

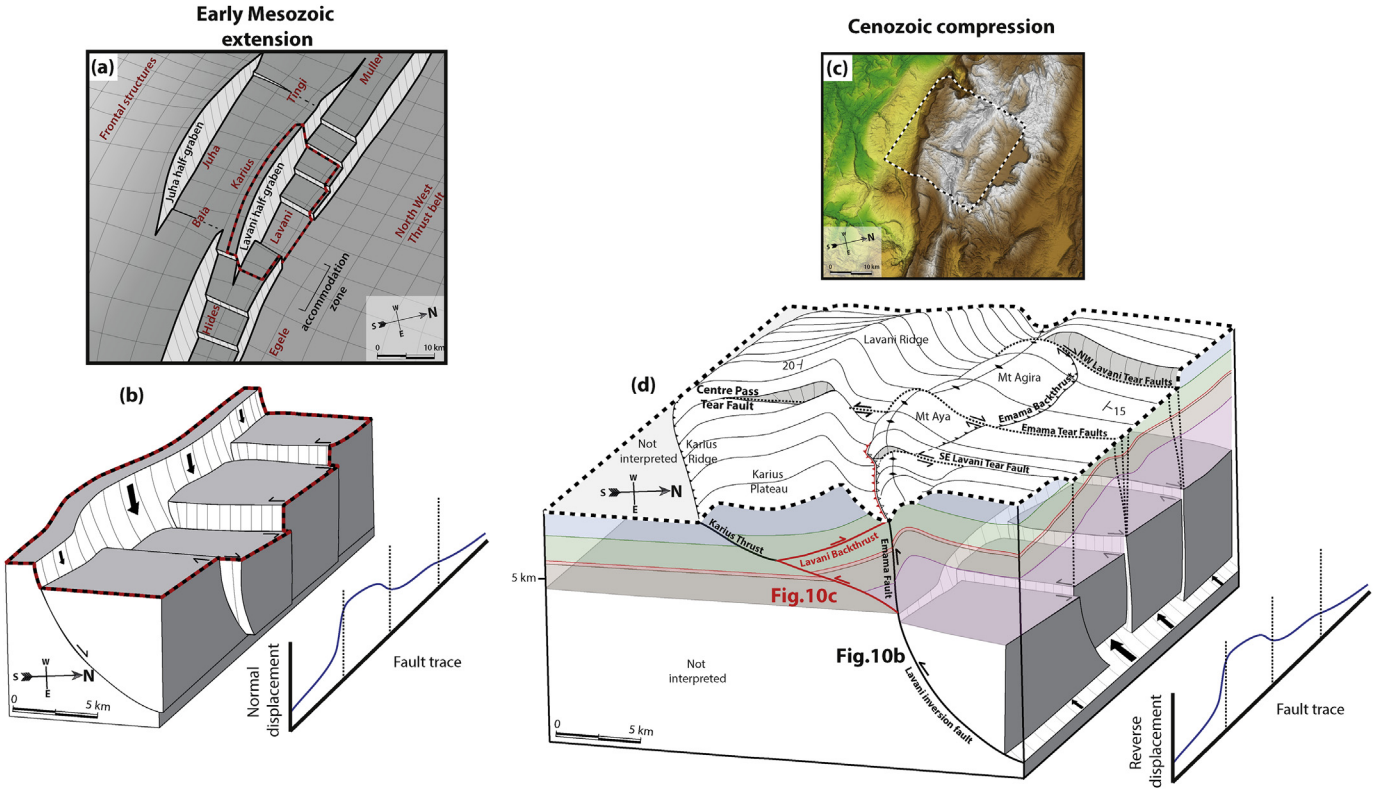

Fig. 11. Model of the 3D evolution of the Eastern Muller Ranges, (a) Schematic Early Mesozoic rift architecture beneath the Greater Juha area with red labels marking the location of present day structural features; (b) Schematic Early Mesozoic rift architecture beneath the Lavani Valley showing the Lavani normal fault, southeast-dipping relay ramp and cross-cutting normal structures. Location marked by dashed red box in (a); (c) SRTM DEM across the Eastern Muller Ranges (USGS, 2015); (d) Cenozoic inversion to form the eastern Muller Ranges, including basement-connected tear faults with opposing movement sense to original cross-cutting normal structures. Note: Mt Aya is simplified by showing its pre-erosion geometry – i.e. shown prior to the erosion of the forelimb of the Lavani Anticline and associated surface exposure of Toro Sandstone and Imburu Mudstone. Location marked by dashed box in (c). (For interpretation of the references to colour in this figure legend, the reader is referred to the web version of this article.)

We suggest the inversion of pre-existing rift architecture is the primary influence on the evolution of the Greater Juha area. A number of prominent detachment-levels have been recognised within the Mesozoic sedimentary sequence in the KFTB (e.g., Hill et al., 2008, 2010), but their relationship with basement-inversion structures has often been unclear. In the Greater Juha area, thrust structures detach from similar horizons (e.g., Cecilia Anticline, Karius Thrust, both detached in the Ieru Formation) but with better-constrained connections to nearby inversion structures. For instance, the extensive and relatively undeformed backlimb of the Lavani Anticline suggests that thrust structures (including triangle zones) across the EMR (e.g., Karius Thrust, Lavani Backthrust) are proximally linked to the steep Lavani inversion fault, rather than distally to structures within the neighbouring North West Thrust Belt (Fig. 1c). Basement-connected triangle zones have been identified in other fold and thrust belts (e.g., Zapata and Allmendinger, 1996; Sterne, 2006), but in general appear less abundant than triangle zones with prominent sedimentary detachments (e.g., floor thrusts). The evolution of triangle zones within the Greater Juha area is likely to be controlled by competence contrasts within the stratigraphic column, in particular between: (1) competent crystalline basement, (2) largely incompetent Early Mesozoic sediments and (3) competent Darai Limestone. Perhaps the best documented analogue for this structure style is the Ellesmerian mountain front in North Greenland. There, balanced cross-sections reveal steeply-dipping, basement-connected inversion structures that connect to a major roof backthrust at the base of a thick carbonate shelf sequence, thus similarly forming triangle zones within the enclosed incompetent basinal sediments, and an elevated mountain front monocline (Soper and Higgins, 1990). Given access and logistical challenges in the PFB, identifying analogues from better understood fold and thrust belts worldwide is likely to be crucial to improve our understanding of sub-surface structure.

Also, robust geochronological data are required to constrain the temporal evolution of the Greater Juha area and to help develop kinematic and mechanical structural models. Furthermore, additional modelling is required to understand: (1) why the generally similar Lavani and Juha anticlines differ in having an emergent frontal fault (Emama Fault) and blind frontal fault (Juha inversion fault), respectively, and; (2) the geometric evolution of the Lavani inversion fault from the steep-dipping Emama Fault to shallowly-dipping detachments and thrust structures within the sedimentary sequence.

6.2. Arc-normal lineaments and structures

Arc-normal oriented structures are pervasive across a range of scales within the Greater Juha area of the PFB. We suggest this observed trend relates directly to zones of tear faulting that connect at depth to weakened pre-existing basement cross-structures that have inverted during compression to accommodate lateral displacement variations (Fig. 11d). The dominant movement sense along arc-normal structures is oblique dextral, up-to-the-southeast, consistent with structures also observed within the KFTB (Hill et al., 2008, 2010), the Hides Anticline (Johnstone and Emmett, 2000), between the Cecilia, Wai Asi and Strickland

Anticlines (Craig and Warvakai, 2009), in the EMR (e.g., Legari Tear; Hornafius, 1993), WMR (Eisenberg, 1996) and in the WPFB (White et al., 2014). Regional-scale arc-normal lineaments are also commonly associated with dextral offset, including the Bosavi Lineament (e.g., Osborne, 1990) and a lineament interpreted to run through the Strickland Gorge (Hill, 1989) (Fig. 1b).

Observations from geological data across the Greater Juha area highlight the secondary presence of arc-normal structures with oblique sinistral, up-to-the-northwest movement sense (e.g., Figs. 4a and 11d). We found no convincing evidence of regionally-continuous arc-normal lineaments intersecting the Greater Juha area regionally. This suggests that regional-scale lineaments observed across the PFB may consist of less continuous, smaller-scale arc-normal structures and thus may not necessarily relate to regional-scale rift architecture (i.e. transfer faults). For instance, arc-normal structures across Lavani Valley appear to be basement-connected, but discontinuous, as they do not appear to disturb the backlimb of the Lavani Anticline and Lavani Ridge. Even the apparently continuous Emama Tear Faults and Centre Pass Tear Fault appear to have differing movement senses (Fig. 6b). We suggest the Emama Tear Faults relate to foreland-vergent inversion along the underlying Lavani normal fault, while the Centre Pass Tear Fault relates to hinterland-vergent thrusting along the Lavani Backthrust, and thus the latter is not directly related to an underlying basement structure (Fig. 11d). This highlights the importance of understanding the relationship between arc-parallel structural style and arc-normal structures, something that is often overlooked during cross-section based studies.

The controls on, and relationships between, local-scale arc-normal structures and regional-scale arc-normal lineaments within the PFB are largely unclear, but are likely to be complex. Early Mesozoic rift architecture is clearly influencing lateral variations in structural style across the PFB (e.g., Hill, 1991; Hill et al., 2010) however arc-normal structures and lineaments that appear to accommodate this variation may ultimately relate to a complex basement fabric beneath the PFB with an overall northeast to southwest orientation (e.g., White et al., 2014).

The influence of basement fabrics on rift architecture (e.g., Smith and Mosley, 1993; Ring, 1994; Corti et al., 2007) and subsequent inversion (e.g., Piquer et al., 2016) is well-established elsewhere. Thus, it is plausible that Palaeozoic basement fabric controlled the structural framework of the Papuan Basin during rifting in the Early Mesozoic, forming regional-scale accommodation zones and related local-scale transfer structures that are now expressed as regional-scale arc-normal lineaments and local-scale arc-normal structures, respectively. Transfer structures, including complexly breached relay ramps, utilise northeast-southwest striking weaknesses associated with the basement fabric, as a mechanism for accommodating displacement along major northwest-southeast striking normal faults (e.g., Fig. 11a). These structures have subsequently been inverted to form arc-normal oriented zones of tear faulting that accommodate laterally variable displacement along inversion faults and connected thrust structures. Additional work should focus on developing a more robust understanding of the relationship between basement fabric, Early Mesozoic rift architecture and subsequent Cenozoic inversion, and the 3D spatio-temporal evolution of the PFB.

Acknowledgments

This work was funded by Papuan Oil Search Ltd and ExxonMobil through their PPL402 joint venture. Luke Mahoney acknowledges support of an Australian Postgraduate Award. Many thanks to Tony Allan and Tony Norman who were colleagues and mentors during the Greater Juha Geological Survey. Midland Valley Exploration kindly provided the Move software suite as a part of their Academic Software Initiative. We appreciate comments and suggestions from Hugh Davies and Mark Cooper.

Appendix A. Supplementary data

Supplementary data related to this article can be found at http://dx.doi.org/10.1016/j.jsg.2017.05.010.

References

Abers, G., McCaffrey, R., 1988. Active deformation in the New Guinea fold-and-thrust belt: seismological evidence for strike-slip faulting and basement-involved thrusting. J. Geophys. Res. Solid Earth 93, 13332–13354.
Allan, T.L., Trotter, J.A., Whitford, D.J., Korsch, M.J., 2000. Strontium isotope stratigraphy and the oligocene-miocene T-letter "stages" in Papua New Guinea. In: Buchanan, P., Grainge, A., Thornton, R. (Eds.), Petroleum Exploration, Development, and Production in Papua New Guinea: Proceedings of the Fourth PNG Petroleum Convention. Papua New Guinea Chamber of Mines and Petroleum, Port Moresby, pp. 155–168.
Amoco PNG Exploration Company, 1982. Lavani 1 Well Completion Report, p. 137.
Baldwin, S., Fitzgerald, P., Webb, L., 2012. Tectonics of the new Guinea region. Annu. Rev. Earth Planet. Sci. 40, 495–520.
Bennett, D.J., Brand, R.P., Mills, C.R., Morris, B.D., 2000. Exploration potential of the West Bosavi area, Papuan foreland basin, Papua New Guinea. In: Buchanan, P., Grainge, A., Thornton, R. (Eds.), Petroleum Exploration, Development, and Production in Papua New Guinea: Proceedings of the Fourth PNG Petroleum Convention. Papua New Guinea Chamber of Mines and Petroleum, Port Moresby, pp. 139–154.
Bidstone, B.J., St. John, V.P., Thomas, E.G., 1974. Report on the Lavani Valley Seismic and Gravity Survey, Geological Survey of Papua New Guinea Archive File F1/S/74–21 (unpubl.).
Bonini, Marco, Sani, Federico, Antonielli, Benedetta, 2012. Basin inversion and contractional reactivation of inherited normal faults: a review based on previous and new experimental models. Tectonophysics 522–523, 55–88.
Bradley, G., 2014. Western Papuan Basin to Western Aure: Generalised Cenozoic - Jurassic Chronostratigraphy (unpubl.), p. 1.
Buchanan, J.G., Buchanan, P.G. (Eds.), 1995. Basin inversion. Geological Society, London, Special Publications 88.
Buchanan, P., Warburton, J., 1996. The influence of pre-existing basin architecture in the development of the Papuan fold and thrust belt: implications for petroleum prospectivity. In: Buchanan, P. (Ed.), Petroleum Exploration, Development, and Production in Papua New Guinea: Proceedings of the Third PNG Petroleum Convention. Papua New Guinea Chamber of Mines and Petroleum, Port Moresby, pp. 89–109.
Chorowicz, Jean, 2005. The East African rift system. J. Afr. Earth Sci. 43 (1–3), 379–410.
Cooper, M., 1996. Passive-roof duplexes and pseudo-passive-roof duplexes at mountain fronts: a review. Bull. Can. Petrol. Geol. 44, 410–421.
Corbett, G., 1994. Regional structural control of selected Cu/Au occurrences in Papua New Guinea. In: Rogerson, R. (Ed.), Proceedings of the PNG Geology, Exploration and Mining Conference 1994. Australasian Institute of Mining and Metallurgy, pp. 57–70.
Corti, Giacomo, van Wijk, Jolante, Cloetingh, Sierd, Morley, Chris K., 2007. Tectonic inheritance and continental rift architecture: numerical and analogue models of the East African Rift system. Tectonics 26 (6), n/a-n/a.
Craig, M.S., Warvakai, K., 2009. Structure of an active foreland fold and thrust belt, Papua New Guinea. Aust. J. Earth Sci. 56 (5), 719–738.
Crowhurst, P., Hill, K., Foster, D., 1997. The structural and tectonic development of the Frieda River Mineral district, NW Papua New Guinea. In: Hancock, G. (Ed.), Proceedings of the PNG Geology, Exploration and Mining Conference 1997. Australasian Institute of Mining and Metallurgy, pp. 51–60.
Davies, H., 1983. Wabag 1:250 000 Geological Series Explanatory Notes Sheet SB/54-8. Geological Survey of Papua New Guinea, PNG Department of Minerals and Energy, Port Moresby.
Davies, H., 1991. Regional geologic setting of some mineral deposits of the New Guinea region. In: Rogerson, R. (Ed.), Proceedings of the Papua New Guinea Geology, Exploration and Mining Conference 1991. Australasian Institute of Mining and Metallurgy, pp. 49–57.
Davies, H., Norvick, M., 1974. Blucher Range 1:250 000 Geological Series Explanatory Notes Sheet SB/54-07. Geological Survey of Papua New Guinea, PNG Department of Minerals and Energy, Port Moresby.
Denison, C.N., 1990. Palynostratigraphic Revision of Amoco Lavani-1 Well, Papua New Guinea (unpubl.), p. 6.
Eisenberg, L.I., 1996. Strontium isotope analysis and structural interpretation of P'nyang Anticline, Papuan Fold belt, Western Highlands Province, Papua New Guinea. In: Buchanan, P. (Ed.), Petroleum Exploration, Development, and Production in Papua New Guinea: Proceedings of the Third PNG Petroleum Convention. Papua New Guinea Chamber of Mines and Petroleum, Port Moresby, pp. 231–244.
Eisenstadt, G., Withjack, M.O., 1995. Estimating Inversion: Results from Clay

Models. Geological Society, London, Special Publications 88, pp. 119–136.
Ekström, G., Nettles, M., Dziewoński, A.M., 2012. The global CMT project 2004–2010: centroid-moment tensors for 13,017 earthquakes. Phys. Earth Planet. Inter. 200–201, 1–9.
Fossen, Haakon, Rotevatn, Atle, 2016. Fault linkage and relay structures in extensional settings—a review. Earth Sci. Rev. 154, 14–28.
Frankowicz, E., McClay, K.R., 2010. Extensional fault segmentation and linkages, Bonaparte Basin, outer North West Shelf, Australia. Bulletin 94 (7), 977–1010.
Gow, P.A., Upton, P., Zhao, C., Hill, K.C., 2002. Copper-gold mineralisation in New Guinea: numerical modelling of collision, fluid flow and intrusion-related hydrothermal systems. Aust. J. Earth Sci. 49 (4), 753–771.
Gupta, Anupma, Scholz, Christopher H., 2000. A model of normal fault interaction based on observations and theory. J. Struct. Geol. 22 (7), 865–879.
Hall, Robert, 1996. Reconstructing cenozoic SE Asia. Geol. Soc. Lond. Spec. Publ. 106 (1), 153–184.
Hall, R., 1997. Cainozoic tectonics of SE Asia and Australia. In: Howes, J., Noble, R. (Eds.), Proceedings of the International Conference on Petroleum Systems of SE Asia and Australia. Indonesian Petroleum Association, Jakarta, pp. 47–62.
Hall, Robert, 2002. Cenozoic geological and plate tectonic evolution of SE Asia and the SW Pacific: computer-based reconstructions, model and animations. J. Asian Earth Sci. 20 (4), 353–431.
Hall, Robert, 2012. Late Jurassic–cenozoic reconstructions of the Indonesian region and the Indian Ocean. Tectonophysics 570–571, 1–41.
Hanani, A., Lennox, P., Hill, K.C., 2016. The geology and structural style of the Juha gas field, Papua New Guinea. ASEG Ext. Abstr. 2016, 1–7.
Hill, Kevin C., 1989. The Muller anticline, Papua New Guinea; basement-cored, inverted extensional fault structures with opposite vergence. Tectonophysics 158 (1–4), 227–245.
Hill, K.C., 1991. Structure of the Papuan Fold belt, Papua New Guinea. Am. Assoc. Petrol. Geol. Bull. 75, 857–872.
Hill, K.C., Bradey, K., Iwanec, J., Wilson, N., Lucas, K., 2008. Structural exploration in the Papua New Guinea Fold Belt. In: Blevin, J.E., Bradshaw, B.E., Uruski, C. (Eds.), Eastern Australian Basins Symposium III, Petroleum Exploration Society of Australia, Special Publication 225238.
Hill, K.C., Gleadow, A.J.W., 1989. Uplift and thermal history of the Papuan Fold Belt, Papua New Guinea: apatite fission track analysis. Aust. J. Earth Sci. 36 (4), 515–539.
Hill, K.C., Hall, R., 2003. Mesozoic-Cenozoic evolution of Australia's New Guinea margin in a west Pacific context. Geol. Soc. Am. Special Pap. 372, 265–290.
Hill, K.C., Kendrick, R.D., Crowhurst, P.V., Gow, P.A., 2002. Copper-gold mineralisation in New Guinea: tectonics, lineaments, thermochronology and structure. Aust. J. Earth Sci. 49 (4), 737–752.
Hill, K.C., Lucas, K., Bradey, K., 2010. Structural styles in the Papuan Fold Belt, Papua New Guinea: constraints from analogue modelling. In: Goffey, G. (Ed.), Hydrocarbons in Contractional Belts. Geological Society, London, pp. 33–56. Special Publications 348.
Hill, K.C., Norvick, M., Keetley, J., Adams, A., 2000. Structural and stratigraphic shelf-edge hydrocarbon plays in the Papuan Fold Belt. In: Buchanan, P., Grainge, A., Thornton, R. (Eds.), Petroleum Exploration, Development, and Production in Papua New Guinea: Proceedings of the Fourth PNG Petroleum Convention. Papua New Guinea Chamber of Mines and Petroleum, Port Moresby, pp. 67–85.
Hill, G.S., Price, S.J., Foster, M.S., Stephenson, R.W., Ellis, D., Lyslo, J.A., 1996a. Seismic acquisition in the Papuan Fold belt – a new approach. In: Buchanan, P. (Ed.), Petroleum Exploration, Development, and Production in Papua New Guinea: Proceedings of the Third PNG Petroleum Convention. Papua New Guinea Chamber of Mines and Petroleum, Port Moresby, pp. 445–458.
Hill, Kevin C., Raza, Asaf, 1999. Arc-continent collision in Papua Guinea: constraints from fission track thermochronology. Tectonics 18 (6), 950–966.
Hill, K.C., Simpson, R., Kendrick, R., Crowhurst, P., O'Sullivan, P., Saefudin, I., 1996b. Hydrocarbons in New Guinea, controlled by basement fabric, Mesozoic extension and Tertiary Convergent margin tectonics. In: Buchanan, P. (Ed.), Petroleum Exploration, Development, and Production in Papua New Guinea: Proceedings of the Third PNG Petroleum Convention. Papua New Guinea Chamber of Mines and Petroleum, Port Moresby, pp. 63–76.
Hobson, D.M., 1986. A thin-skinned model for the Papuan thrust belt and some implications for hydrocarbon exploration. Aust. Petrol. Explor. Assoc. J. 26, 214–224.
Home, P., Dalton, D., Brannan, J., 1990. Geological evolution of the Western Papuan Basin. In: Carman, G., Carman, Z. (Eds.), Petroleum Exploration, Development, and Production in Papua New Guinea: Proceedings of the First PNG Petroleum Convention. Papua New Guinea Chamber of Mines and Petroleum, Port Moresby, pp. 107–118.
Hornafius, J.S., 1993. The 1990-1991 Muller Range Geological Survey – PPL 93. Mobil Exploration Niugini (unpubl.).
Hornafius, J.S., Denison, R.E., 1993. Structural interpretations based on strontium isotope dating of the Darai limestone, Papuan Fold belt, new Guinea. In: Carman, G., Carman, Z. (Eds.), Petroleum Exploration, Development, and Production in Papua New Guinea: Proceedings of the Second PNG Petroleum Convention. Papua New Guinea Chamber of Mines and Petroleum, Port Moresby, pp. 313–324.
Hus, R., Acocella, V., Funiciello, R., De Batist, M., 2005. Sandbox models of relay ramp structure and evolution. J. Struct. Geol. 27 (3), 459–473.
Jenkins, D., 1974. Detachment tectonics in western Papua New Guinea. Geol. Soc. Am. Bull. 85, 533–548.
Jenkins, D., White, M.F., 1970. Report on the Strickland River Survey, Permit 46, Papua New Guinea. BP Petroleum Development Australian Pty Ltd. Geological survey of Papua New Guinea archive file 4 BS (unpubl.).
Johnstone, D., Emmett, J., 2000. Petroleum geology of the Hides gas field, southern Highlands, Papua New Guinea. In: Buchanan, P., Grainge, A., Thornton, R. (Eds.), Petroleum Exploration, Development, and Production in Papua New Guinea: Proceedings of the Fourth PNG Petroleum Convention. Papua New Guinea Chamber of Mines and Petroleum, Port Moresby, pp. 319–335.
Jones, P.B., 1996. Triangle zone geometry, terminology and kinematics. Bull. Can. Petrol. Geol. 44, 139–152.
Kawagle, S.A., Meyers, J.B., 1996. Structural and sequence geometry of the Kiunga area, Papuan foreland basin, Papua New Guinea. In: Buchanan, P. (Ed.), Petroleum Exploration, Development, and Production in Papua New Guinea: Proceedings of the Third PNG Petroleum Convention. Papua New Guinea Chamber of Mines and Petroleum, Port Moresby, pp. 175–193.
Keenan, S.E., Hill, K.C., 2015. The Mananda Anticline, Papua New Guinea: a third oil discovery, appraisal programme and deep potential. In: AAPG/SEG International Conference and Exhibition 2015.
Kelly, P.G., Peacock, D.C.P., Sanderson, D.J., McGurk, A.C., 1999. Selective reverse-reactivation of normal faults, and deformation around reverse-reactivated faults in the Mesozoic of the Somerset coast. J. Struct. Geol. 21 (5), 493–509.
Koulali, A., Tregoning, P., McClusky, S., Stanaway, R., Wallace, L., Lister, G., 2015. New Insights into the present-day kinematics of the central and western Papua New Guinea from GPS. Geophys. J. Int. 202 (2), 993–1004.
Löffler, E., MacKenzie, D., Webb, A., 1979. Potassium-argon ages from some of the Papua New Guinea Highlands volcanoes, and their relevance to Pleistocene geomorphic history. J. Geol. Soc. Aust. 26, 387–397.
Longley, I.M., Buessenschuett, C., Clydsdale, L., Cubitt, C.J., Davis, R.C., Johnson, M.K., Marshall, N.M., Murray, A.P., Somerville, R., Spry, T.B., Thompson, N.B., 2002. The North West Shelf of Australia–a woodside perspective. Sediment. Basins West. Aust. 3, 27–88.
Lunt, P., Allan, T., 2004. Larger foraminifera in Indonesian biostratigraphy, calibrated to isotopic dating. In: GRDC Museum Workshop on Micropalaeontology. Bandung 1–109.
McClay, K.R., 1995. The geometries and kinematics of inverted fault systems: a review of analogue model studies. Geological Society, London, Special Publications 88, pp. 97–118.
McConachie, B., Lanzilli, E., Kendrick, D., Burge, C., 2000. Extensions of the Papuan Basin Foreland geology into Eastern Irian Jaya (West Papua) and the new Guinea Fold Belt in Papua New Guinea. In: Buchanan, P., Grainge, A., Thornton, R. (Eds.), Petroleum Exploration, Development, and Production in Papua New Guinea: Proceedings of the Fourth PNG Petroleum Convention. Papua New Guinea Chamber of Mines and Petroleum, Port Moresby, pp. 219–238.
Medd, D.M., 1996. Triangle zone deformation at the leading edge of the Papuan Fold Belt. In: Buchanan, P. (Ed.), Petroleum Exploration, Development, and Production in Papua New Guinea: Proceedings of the Third PNG Petroleum Convention. Papua New Guinea Chamber of Mines and Petroleum, Port Moresby, pp. 217–229.
Metcalfe, I., 2002. Permian tectonic framework and palaeogeography of SE Asia. J. Asian Earth Sci. 20 (6), 551–566.
Mobil Exploration Niugini, 1991. Muller 1X Well Completion Report, p. 58.
Morley, C.K., Nelson, R.A., Patton, T.L., Munn, S.G., 1990. Transfer zones in the East African rift system and their relevance to hydrocarbon exploration in rifts. Am. Assoc. Petrol. Geol. Bull. 74, 1234–1253.
Muraoka, Hirofumi, Kamata, Hiroki, 1983. Displacement distribution along minor fault traces. J. Struct. Geol. 5 (5), 483–495.
Niugini Gulf Oil Pty Ltd, 1983. Juha 1 Well Completion Report, p. 77.
Osborne, D.G., 1990. The hydrocarbon potential of the western Papuan Basin foreland—with reference to worldwide analogues. In: Carman, G., Carman, Z. (Eds.), Petroleum Exploration, Development, and Production in Papua New Guinea: Proceedings of the First PNG Petroleum Convention. Papua New Guinea Chamber of Mines and Petroleum, Port Moresby, pp. 197–213.
Page, R., 1976. Geochronology of igneous and metamorphic rocks in the New Guinea Highlands. Bureau Miner. Resour. Aust. Bull. 162, 117.
Panien, Marion, Schreurs, Guido, Pfiffner, Adrian, 2005. Sandbox experiments on basin inversion: testing the influence of basin orientation and basin fill. J. Struct. Geol. 27 (3), 433–445.
Peacock, D.C.P., Sanderson, D.J., 1991. Displacements, segment linkage and relay ramps in normal fault zones. J. Struct. Geol. 13 (6), 721–733.
Pigott, J.D., Trumbly, N.I., O'Neal, M.V., 1985. Northern New Guinea wrench fault system: a manifestation of Late Cenozoic interactions between Australian and Pacific plates. Tectonics 4, 613–620.
Pigram, C.J., Panggabean, H., 1984. Rifting of the northern margin of the Australian continent and the origin of some microcontinents in Eastern Indonesia. Tectonophysics 107 (3–4), 331–353.
Pigram, C.J., Symonds, P.A., 1991. A review of the timing of the major tectonic events in the New Guinea Orogen. J. Southeast Asian Earth Sci. 6 (3–4), 307–318.
Piquer, Jose, Berry, Ron F., Scott, Robert J., Cooke, David R., 2016. Arc-oblique fault systems: their role in the Cenozoic structural evolution and metallogenesis of the Andes of central Chile. J. Struct. Geol. 89, 101–117.
Reilly, C., Nicol, A., Walsh, J., 2016. Importance of Pre-existing Fault Size for the Evolution of an Inverted Fault System. Geological Society, London, Special Publications 439. SP439–2.
Ring, Uwe, 1994. The influence of preexisting structure on the evolution of the Cenozoic Malawi rift (East African rift system). Tectonics 13 (2), 313–326.

Saintot, Aline, Angelier, Jacques, 2002. Tectonic paleostress fields and structural evolution of the NW-Caucasus fold-and-thrust belt from Late Cretaceous to Quaternary. Tectonophysics 357 (1–4), 1–31.
Schofield, S., 2000. The Bosavi arch and the Komewu fault zone: their control on basin architecture and the prospectivity of the Papuan foreland. In: Buchanan, P., Grainge, A., Thornton, R. (Eds.), Petroleum Exploration, Development, and Production in Papua New Guinea: Proceedings of the Fourth PNG Petroleum Convention. Papua New Guinea Chamber of Mines and Petroleum, Port Moresby, pp. 101–122.
Smith, R.I., 1990. Tertiary plate tectonic setting and evolution of Papua New Guinea. In: Carman, G., Carman, Z. (Eds.), Petroleum Exploration, Development, and Production in Papua New Guinea: Proceedings of the First PNG Petroleum Convention. Papua New Guinea Chamber of Mines and Petroleum, Port Moresby, pp. 229–244.
Smith, Martin, Mosley, Peter, 1993. Crustal heterogeneity and basement influence on the development of the Kenya Rift, East Africa. Tectonics 12 (2), 591–606.
Soliva, Roger, Benedicto, Antonio, 2004. A linkage criterion for segmented normal faults. J. Struct. Geol. 26 (12), 2251–2267.
Soper, N.J., Higgins, A.K., 1990. Models for the Ellesmerian mountain front in North Greenland: a basin margin inverted by basement uplift. J. Struct. Geol. 12 (1), 83–97.
Stanaway, R., Noonan, J., 2015. Geodetic measurement of deformation within the Papuan Fold and thrust belt. In: American Association of Petroleum Geologists International Conference and Exhibition, 13th-16th September 2015, Melbourne, Australia.
Sterne, E.J.N., 2006. Stacked,“evolved” triangle zones along the southeastern flank of the Colorado Front Range. Mt. Geol. 43, 65–92.
Storti, F., McClay, K., 1995. Influence of syntectonic sedimentation on thrust wedges in analogue models. Geology 23, 999–1002.
Suppe, J., 1980. Imbricated structure of western foothills belt, southcentral Taiwan. Petrol. Geol. Taiwan 17, 1–16.
Texaco Overseas Petroleum Company, 1971. Cecilia 1 Well Completion Report, p. 130.
Thornton, R., Emmett, J., Laslo, J., Gottschalk, R., 1996. Integrated structural and stratigraphic analysis in PPL 175, Papuan Fold belt, Papua New Guinea. In: Buchanan, P. (Ed.), Petroleum Exploration, Development, and Production in Papua New Guinea: Proceedings of the Third PNG Petroleum Convention. Papua New Guinea Chamber of Mines and Petroleum, Port Moresby, pp. 195–215.
Trudgill, B., Cartwright, J., 1994. Relay-ramp forms and normal-fault linkages, Canyonlands National Park, Utah. Geol. Soc. Am. Bull. 106, 1143–1157.
USGS, 2015. Shuttle Radar Topography Mission, 1-arc Second, Global Land Cover Facility, University of Maryland, College Park, Maryland. Accessed through USGS EarthExplorer.
Wallace, Laura M., Stevens, Colleen, Silver, Eli, McCaffrey, Rob, Loratung, Wesley, Hasiata, Suvenia, Stanaway, Richard, Curley, Robert, Rosa, Robert, Taugaloidi, Jones, 2004. GPS and seismological constraints on active tectonics and arc-continent collision in Papua New Guinea: implications for mechanics of microplate rotations in a plate boundary zone. J. Geophys. Res. 109 (B5).
Webb, A., 1973. Geochronology Report on Samples Submitted by BMR West Sepik Party. Australian Mineral Development Laboratories Report AN3049/73 (unpubl.).
White, M.F., Marfleet, M.J., 1973. Laigap Geological Survey, Permit 46, Papua New Guinea. BP Petroleum Development Australian Pty Ltd. Geological survey of Papua New Guinea archive file 13 BL (unpubl.).
White, L.T., Morse, M.P., Lister, G.S., 2014. Lithospheric-scale structures in New Guinea and their control on the location of gold and copper deposits. Solid Earth 5 (1), 163–179.
Zahirovic, S., Seton, M., Müller, R.D., 2014. The cretaceous and cenozoic tectonic evolution of southeast Asia. Solid Earth 5 (1), 227–273.
Zahirovic, S., Matthews, K.J., Flament, N., Müller, R.D., Hill, K.C., Seton, M., Gurnis, M., forthcoming, 2016. Tectonic evolution and deep mantle structure of eastern Tethyan domain since the latest Jurassic. Earth Sci. Rev. 162, 293–337.
Zapata, T.R., Allmendinger, R.W., 1996. Thrust-front zone of the Precordillera, Argentina: a thick-skinned triangle zone. Am. Assoc. Petrol. Geol. Bull. 80, 359–381.